

Measurements of Thermal Structure and Thermal Contrasts in the Atmosphere of Venus and Related Dynamical Observations: Results From the Four Pioneer Venus Probes

A. SEIFF,¹ DONN B. KIRK,¹ RICHARD E. YOUNG,¹ ROBERT C. BLANCHARD,²
JOHN T. FINDLAY,³ G. M. KELLY,³ AND S. C. SOMMER¹

Thermal structure of the atmosphere of Venus, and differences in structure with latitude (up to 60°) and clock hour (from midnight to 8 A.M.) have been measured in situ from an altitude of 126 km to the surface by instruments on the four Pioneer Venus entry probes. Several indications from the preliminary analyses are confirmed by the current analysis: Thermal contrasts below 45 km are a few K, with the mid-latitudes warmer than both equatorial and the high latitudes. Sizeable temperature and pressure differences with latitude develop in the clouds (25 K and 20 mbar at the 200 mbar level). At 30° latitude, diurnal differences were small throughout the lower atmosphere from midnight to 7 A.M. A major stable layer 25 km deep exists just below the clouds. Waves of global extent were observed within this layer. A locally stable layer is indicated in the deep atmosphere, between 10 and 20 km, at latitudes up to 30°. In the middle cloud and immediately below the deep stable layer, the atmosphere is approximately neutrally stable, and there is evidence for convective overturning below the stable layer. Just above the clouds, the lapse rate becomes stable, and a 'stratosphere' begins which extends upwards to 110 km, becoming isothermal above 85 km. The stratospheric temperature profiles were essentially the same in three widely separated soundings. Upward of 110 km, there is evidence of large amplitude temperature oscillations with altitude, believed to signify the presence of large amplitude waves, perhaps thermal tides. By comparing data of several experiments, it is found that the large diurnal variations in the upper atmosphere begin at an altitude ~115 km. Agreement of structure data from other Pioneer Venus experiments with the present results is generally excellent. Our measurements of the winds derived from Doppler data agree well with DLBI results and indicate a retrograde zonal velocity of 113 m/s at 63 km altitude and 30° latitude. The zonal winds predicted at cloud levels from pressure differences between 60° latitude and the mid-latitude probes by assumption of cyclostrophic balance are in first order agreement with the observed winds. At latitudes below ~30°, however, cyclostrophic balance of the zonal winds is not the dominant process. At altitudes from 60 to 105 km, the measured pressure differences and the assumption of cyclostrophic balance indicate zonal wind velocities peaking at 155 m/s at 68 km, remaining above 120 m/s up to 95 km, then decreasing rapidly.

INTRODUCTION

The atmosphere structure experiment on the four Pioneer Venus probes made in situ measurements of the atmosphere of Venus from an altitude of 126 km to impact, at four widely separated sites. Preliminary results of these measurements have been reported by Seiff *et al.* [1979a, b].

The purpose of the present paper is to move toward a more complete and definitive statement of the results of this experiment. We will report for the first time on the accurately decalibrated complete set of data taken in descent below 66 km, rather than the hand decalibrated selected points presented earlier. As a consequence, the accuracy and the resolution of the data on state properties, and the altitude definition have been improved. We will present tabular data on the structure measured at the four sites, and update the comparison of the four sets of data to define the differences or contrasts available to drive the general circulation. We will present structure data from 65 to above 120 km obtained by three of the four probes during entry, and use them to examine the effects of differences in latitude and local Venus time on structure of the middle atmosphere, and to make wind velocity inferences. We also present for the first time measurements of horizontal

winds derived from experiment data and Doppler tracking during descent.

We will in addition present and discuss data on the detailed structure which relates to the presence of and effects of the cloud layers, and in particular, will update our findings on the static stability of the atmosphere, including indications of a deep, stable layer lying just below the clouds, and a second, slightly stable layer below 20 km. Observations will be presented which give evidence for waves in the stable layer. We will relate the surface pressures to planetary radius at the four entry sites, by making use of data from the Pioneer Venus radar altimeter experiment [Pettengill *et al.*, 1980]. Comparisons will be made with other Pioneer Venus remote and in situ measurements of the atmosphere structure, and with Venera measurements. Together, the Pioneer Venus experiments define the thermal structure from the surface to ~200 km altitude, and graphs showing the structure over this full depth, and interrelationships of the several experiments will be presented.

We expect to make some further investigations from these data, and to make some further refinements. However, the results presented herein are believed to be close to final.

INSTRUMENT ACCURACY AND RESOLUTION

The data to be presented were acquired during entry and descent of the four Pioneer Venus probes by three kinds of sensors, platinum resistance thermometers, miniature diaphragm pressure cells, and guidance quality accelerometers.

¹ NASA Ames Research Center, Moffett Field, California 94035.

² NASA Langley Research Center, Hampton, Virginia 23665.

³ Analytical Mechanics Associates, Hampton, Virginia 23666.

This paper is not subject to U.S. copyright. Published in 1980 by the American Geophysical Union.

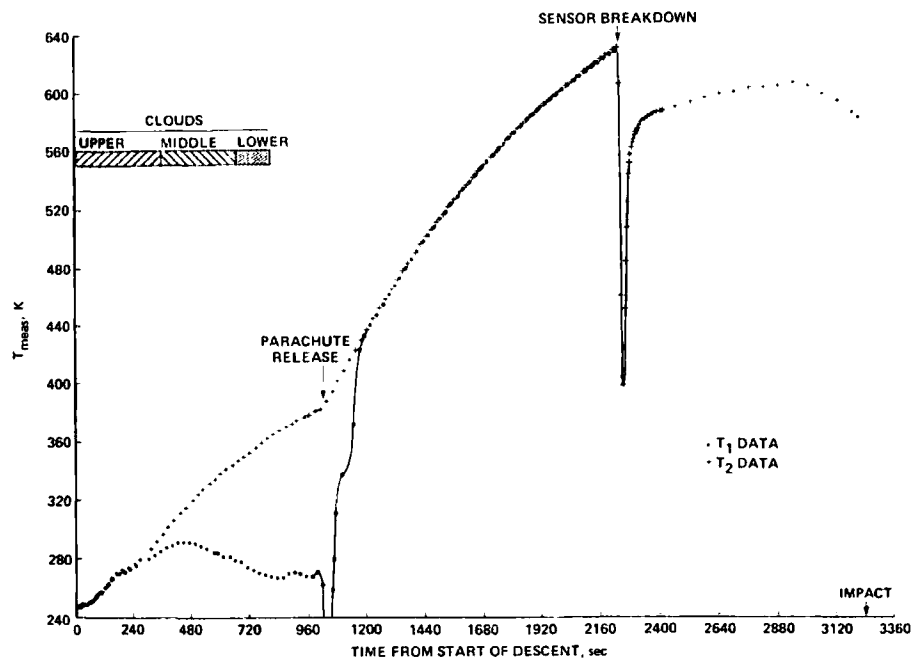


Fig. 1a

Fig. 1. Temperature data received from (a) the sounder and (b) the north probes. In the clouds, the free wire (T_1) sensors were partially shorted to ground by the conducting mist collected on the sensors. Below the clouds, the free wire and bonded sensors came into near agreement until a temperature of 630–640 K was reached, at which point an unidentified phenomenon caused the signal to drop sharply, while simultaneously affecting other probe instruments.

The resistance thermometers and pressure sensors were deployed at the start of the subsonic descent, at 60–66 km altitude, while the accelerometers operated throughout entry and descent, and first sensed the atmosphere at 126 km. We have described these sensors and the complete instrument in more detail in a separate publication [Seiff *et al.*, 1980]. For convenience, we summarize here some key features of the experiment design.

A major goal was to define differences in the structure at the four entry sites. Since these were expected to be small, accuracies of better than 1 K and 0.5% of pressure reading were established as goals. Selected digital resolutions were 0.2 K and 0.2% of full scale on each pressure range.

Two temperature sensing elements were mounted on a single sensing head and read alternately. They were deployed at locations of high fluid velocity to maximize thermal coupling to the atmosphere, and were safely above the probe boundary layers to eliminate convective heat input from the probes. The two measuring elements differed in configuration, and used independent electronics. Hence, they were, in effect, independent sensors, and provided redundancy and accuracy checks. One of the sensors, designated T_1 , was regarded as primary, because of its accuracy advantages. It was a bare platinum wire 0.1 mm in diameter and approximately 1 m long, wrapped in 17.5 turns about an open rectangular frame of platinum rhodium tubing about 2.8 cm on a side. A thin glass film along the frame edges served to insulate the sensing wire from the frame and a second coating over the wires along the frame was used to hold the wires in place. The second sensor, T_2 , was a 0.025 mm diameter \times 6 cm long platinum wire in the form of a raster about 1 cm long by 1 mm high bonded on a film of insulating glass on the outer member of the sensor frame, and covered with a thin glass film to hold it in place [Seiff *et al.*, 1980].

Twelve miniature pressure sensors of progressively increasing range were used to measure pressures from 67 mbar to 95 bars. The 12 sensors provided the necessary wide dynamic range with nearly constant accuracy and resolution. The sensor ranges were geometrically related, each increasing by a factor of approximately 2 over the one preceding, and were alternately assigned to two sets, designated A and B. One sensor from each set was on line at any given time, and the two on-line sensors were read alternately during the descent. This arrangement provided reading checks, accuracy checks, and redundancy. One of the two on-line sensors, the one reading higher in its range, was regarded as primary.

Pre-flight accuracy and stability tests of the pressure sensors showed that the scale factors of the sensors flown were stable within 0.1–0.25% over time periods of 3 months. (The change in scale factors of the 12 sensors on the sounder probe was measured over a 13 month test period encompassing the systems test program, and found to be 0.14% rms.) Zero offsets of the sensors were read just before entry into the atmosphere, and, with temperature corrections where needed, should have been accurate at the time of use within one count or 0.2% of full scale on each range.

Altitude resolution for pressure and temperature was determined by probe descent velocity and sampling frequency, and ranged from about 0.8 km at the start of descent of the small probes to 20 m on the sounder near touchdown.

Scale factor accuracy of the accelerometers was about 0.01%, but was limited on the highest (600 g_E) range (g_E is acceleration of gravity on earth) to about 0.1% by accuracy of calibration of the gain in the instrument electronics. This was better calibrated from the flight data than from the ground tests (to within $\sim 0.025\%$), by requiring probe velocity at the end of the entry period to match that determined independently at the start of descent. Accelerometer bias uncertainties

were o
indepe
taintie:

The
integra
entry.
read o
signed
scale. 1
600 g_E ,
thus li
ranged
time o
riod.

The
peratur
time. F
pressur
and 4.
(every
every
the day
peratur
gence 1
630 K;
630 K.
the sec
third ir
peratur

In th
tially sl
sors be
formed
sulatin;
sensors

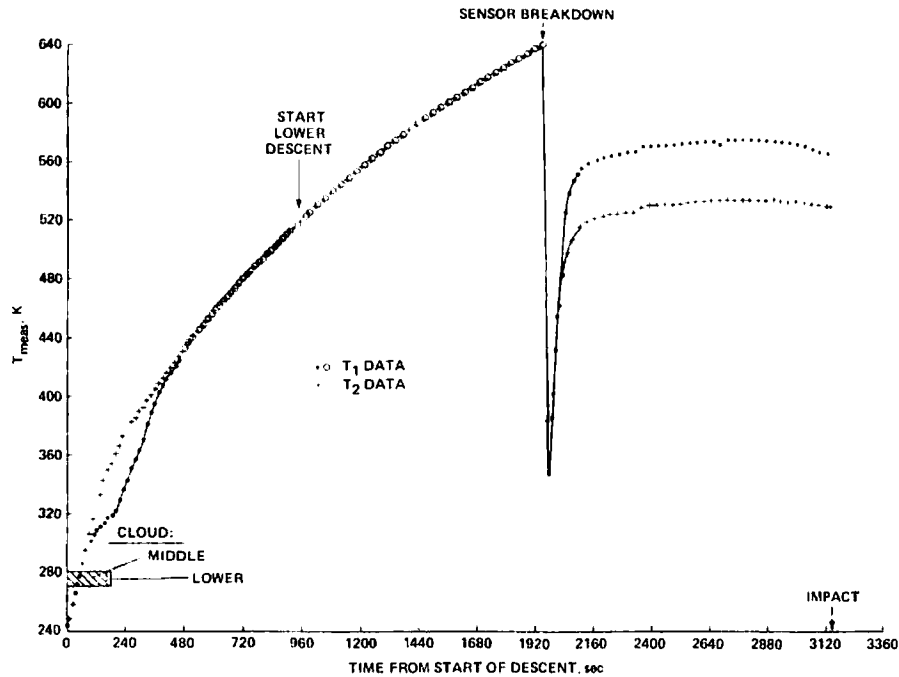


Fig. 1b

were of the order of $5 \times 10^{-5} g_E$ at entry. At impact, based on independent determinations of the planet radius, bias uncertainties were $\approx 10^{-3} g_E$.

The primary sampling mode of the accelerometers was as integrated velocity counts over 0.25 s sampling periods during entry. In descent, integrated velocity change samples were read out at 16 or 8 s intervals. The accelerometers were designed to operate in four ranges, from $10^{-4} g_E$ to $600 g_E$ full scale, but only the higher two ranges, nominally $1.5 g_E$ and $600 g_E$, were acquired in flight. Resolution of acceleration was thus limited to $0.008 g_E$. Altitude resolution during entry ranged from 2.7 km (north probe) to 1.2 km (day probe) at the time of first data, to 0.3 km, and 0.1 km late in the entry period.

PRESENTATION OF DATA

The data acquired were four sets of measurements of temperature, pressure, and velocity increments as functions of time. Representative temperature data are shown in Figure 1; pressure data in Figure 2; and acceleration data in Figures 3 and 4. Figure 1a shows temperatures from the sounder probe (every sixth data point) and Figure 1b, from the north probe (every second data point). Similar data were obtained from the day and night probes. There are three intervals in the temperature data; one from sensor deployment to probe emergence from the clouds; the second from below the clouds to 630 K; and the third, the period of sensor breakdown beyond 630 K. In the first interval, T_1 was affected by the clouds. In the second, the two sensors read in near agreement. In the third interval, between ~ 12 km and the surface, no valid temperature data were acquired.

In the clouds, the T_1 sensors gave evidence of being partially shorted to the sensor frame. This is attributed to the sensors being thoroughly wetted by a conducting mist, which formed conduction paths to ground across the layer of insulating glass on which the sensor wires were wrapped. The T_2 sensors, protected by their glass coatings, were unaffected.

The T_1 shorts start to clear when the probes emerge from the lower cloud. The north probe shorting was minimal, and its descent velocity was high. Thus, clearing of the short began immediately below the clouds, and was rapid. The sounder probe sensor was more severely shorted, and the sounder descent velocity on the parachute was slow, so cloud emergence merely stabilized the T_1 reading. Recovery began at parachute release, when the probe velocity increased to 50 m/s, and was completed within 150 s thereafter. (We believe the droplets were physically removed (blown away) rather than evaporated.)

The sensor breakdown at 630 K has been previously reported [Seiff *et al.*, 1979a]. It was part of an event which affected other small probe instruments [Suomi *et al.*, 1979] and several on the sounder [Colin, this issue]. The breakdown occurred on all four probes at nearly the same atmospheric temperature (630–640 K) and pressure (40 bars), at an altitude of about 12.5 km. The temperature sensor was shown before and after the Venus entries to operate properly in the laboratory at temperatures to 800 K. Possible explanations have been proposed, but not confirmed. One (L. Polaski, private communication, 1979) is that static electrification is involved. For example, it is proposed that a charge is acquired by the probe from atmospheric friction and is discharged at the temperature sensors and net flux radiometers when the probes are deep in the atmosphere. This would be similar to charge accumulation on aircraft in flight, which is discharged through trailing conductors at the wing tips. However, there is no positive identification of the cause of the breakdown.

Pressure sensor data from the sounder and north probes are shown in Figure 2. (Every sixth point is shown from the sounder probe, every third point from the north probe.) Sensor range change times are marked to illustrate the continuity of the data across range changes. The two sensors on line at any given time agree typically within 0.1–1.0%.

Agreement of the A and B set sensors at pressures below 20 bars (altitudes above 20 km) generally supported preflight ac-

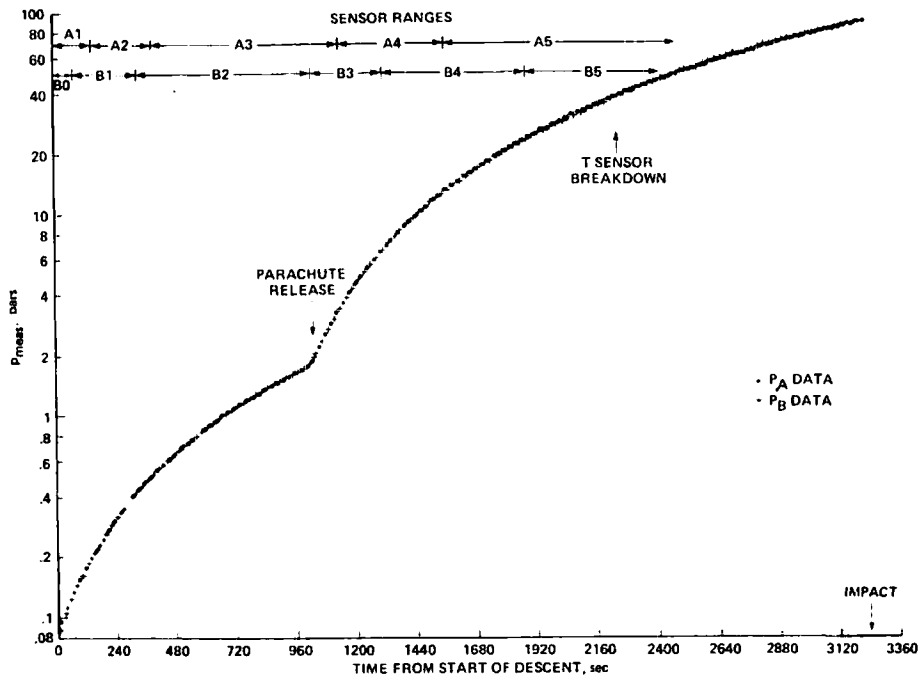


Fig. 2a

Fig. 2. Pressure data from (a) the sounder and (b) the north probes. Agreement between the p_A and p_B sensor sets is generally excellent. Range changes, involving sensor changes, occur as indicated along the top of the chart, and do not disrupt the continuity of the data. In the sounder data the sudden change in dp/dt at 1020 s is due to parachute release and increased fall velocity.

curacy expectations. At pressures above about 20 bars, when diaphragms of lower range sensors broke under pressure load, offset jumps occurred in the data. We attribute these jumps to current leakage in the solid state switches used to select the on-line sensors. The offset jumps were determined accurately where they occurred and were used to correct the subsequent data. Since jumps did not occur simultaneously in the two sensor sets, comparisons between the two were used to confirm that the effect was a pure offset. The data were also tested for changes in slope and curvature across the jumps, and none could be detected. The data from the A and B sensors at the higher pressures generally agreed within 1% for two of the probes, the sounder and the night probe. In the north probe data, above 59 bars, the highest range sensor in the A set, designated A5, showed evidence of drift in the offset and the data therefore were rejected, so only the B5 data are shown. Similarly, the B5 sensor data on the day probe were somewhat erratic at high pressures and were not used. (Although at touchdown of the day probe, B5 read within 0.5 bar of A5, it disagreed with A5 by 1 bar at 33 bars, and exhibited progressive changes in zero offset and reference readings late in the descent.)

The decisions to use redundant sensors and intermittent, in-flight electronics calibration for these measurements thus proved to be invaluable. They permitted us to cope with unforeseen problems as well as to test the accuracy of the measurements.

Acceleration data transmitted by two of the small probes are shown in Figure 3. The north probe experienced a peak deceleration of $459 g_E$ in a main deceleration pulse of only ~ 10 s duration. The sampling rate given to this measurement (4 samples/s, 8 bits per sample) limited the altitude resolution,

but proved to be sufficient to define the density structure of the atmosphere from 64 to 120 km. Better definition of the day probe deceleration pulse was obtained with the same data rate because of the longer pulse duration. (This probe entered the atmosphere less steeply than the north probe.) The sounder probe data are comparable to those from the day probe.

Gaps in the acceleration data were experienced on all the probes after down-ranging from the $600 g_E$ range to the $15 g_E$ range, while the sensor electronics recovered from the switching transient. (Down-ranging actually occurred above $20 g_E$, and the overload lengthened the transient.) Definition of the night probe deceleration pulse was interrupted by a gap of 2.25 s in which the sensor was clearly lagging the rapidly increasing deceleration on the $600 g_E$ range. It has been concluded that this sensor had a defective electronics component which limited the rate of increase of the nulling current. These data have been put aside for later study and will not be reported herein. We believe they will yield some useful results.

Data at the measurement threshold of the day probe are shown in Figure 4. These data are for day probe times earlier than ground received time (GRT) 18:55:52 in Figure 3. The threshold acceleration of -0.08 m/s^2 was defined with small data scatter by summing the velocity pulse counts to define the velocity difference from that at entry. The cumulative velocity change was plotted against time on semilogarithmic paper, on which it defines a line of small curvature, that is, nearly constant slope, owing to the logarithmic increase of atmospheric density. On this graph the threshold is evident from a sudden change in slope. Local slopes define the deceleration through $a_z = (\ln 10) (\Delta V_z) d \log \Delta V_z / dt$, where ΔV_z is the cumulative velocity change. This procedure improves accuracy near threshold and increases threshold altitude, as com-

pared
counts
this pro

ALTITU

Probe
measur
the assu

an integ

where
ature, g
versal g
tor and
of the i
tude z
integra
tables [
by mea
ues of
evaluat

The
accurac
is know
within
do not
nomina
planet
certain
certain
parison
 $\sim 0.45\%$

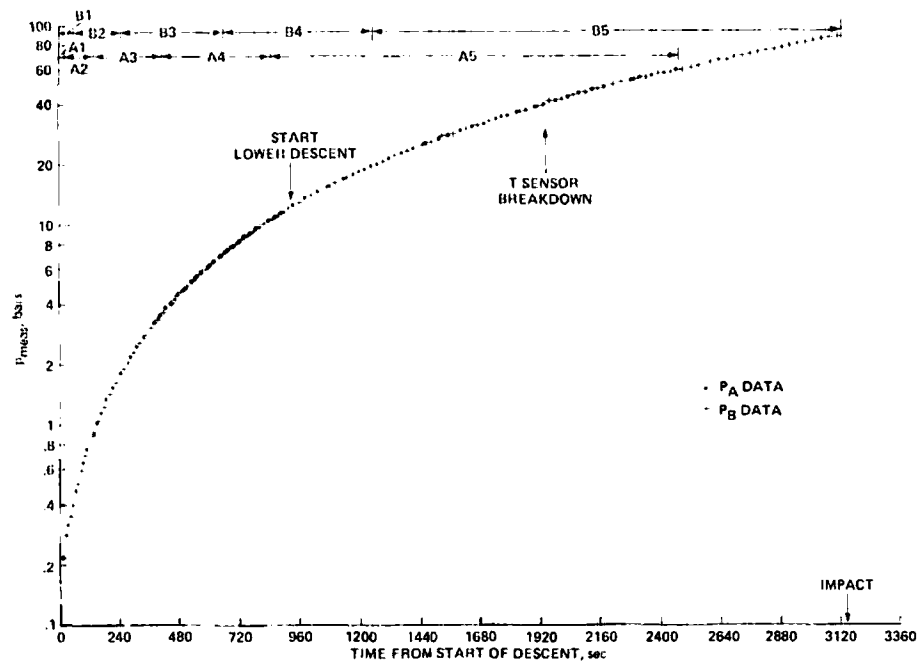


Fig. 2b

pared to computing the accelerations from velocity pulse counts sample by sample. Threshold altitude was 126 km for this probe.

ALTITUDE DEFINITION AND ACCURACY CONSIDERATIONS

Probe altitudes were defined as a function of time from the measurements of temperature and pressure as follows: From the assumption of hydrostatic equilibrium,

$$dp = -\rho g dz \quad (1)$$

an integral to define the altitude is written

$$z = \int_p^{p_0} \frac{\xi RT}{\rho \mu g} dp \quad (2)$$

where p and T are local atmospheric pressure and temperature, $g = g(z)$ is acceleration owing to gravity, R is the universal gas constant, ξ is the imperfect gas compressibility factor and μ is atmospheric mean molecular weight. Evaluation of the integral from the surface to pressure p yields the altitude z above touchdown for the measured p and T . With the integrand defined by the data and values of ξ from the NBS tables [Hilsenrath *et al.*, 1960], the integration was performed by means of a marching quadratic fit to four consecutive values of the integrand. The integral from points 2-3 was then evaluated analytically.

The accuracy of the derived altitudes can be estimated from accuracy of knowledge of factors in the integrand. Thus, if T is known typically to within $\sim 0.2\%$ (1 K at 500 K); dp/p within 1 count (0.4% at midrange) (pressure scale factor errors do not affect altitude, since they affect numerator and denominator equally); g , within 0.008% (0.5 km uncertainty in planet radius at touchdown); and μ , within $\pm 0.2\%$ ($\pm 0.5\%$ uncertainty in N_2 mole fraction), then the root sum square uncertainty in z is $\sim 0.49\%$. For purposes of relative errors (comparisons among probes), the error in μ does not enter and $(\delta z)_{rel} \sim 0.45\%$. The dominant error is the ± 1 count error in pressure

offset, and because we merge the simultaneous data from two sensors and also compare and evaluate the offset errors from readings of each sensor with those which precede and follow it, the error in z may be somewhat less than we have formally indicated, possibly half as great, or 0.25%.

An altitude accuracy test was performed with the sounder data, by evaluating $z(t)$ from p_A and T_1 data, and independently from p_B and T_2 . (It was necessary to substitute T_2 for T_1 in the clouds.) The altitudes disagreed at 64 km by 160 m, or 0.25%; and at 62.25 km by 110 m, or 0.18%, thus tending to support the altitude accuracy estimates given above.

The two independent data sets, T_1 and T_2 , p_A and p_B , were graphically compared and were studied for disagreements and possible offset errors, etc. They were then merged to form a single data set. In the case of the pressure data, the merging consisted of graphically or analytically fitting curves to $p_A(t)$ and to $p_B(t)$ variations such as are shown in Figure 2 and correcting the best fit lines for resolution offset. (Because of finite resolution, curves which best fit the data will represent the mid point of the resolution interval above the count value, whereas the points are the count values. Hence, a correction of $+\frac{1}{2}$ count was applied to the fitted curves.) Preference was then generally given to the primary sensor, that is, the on-line sensor which is higher in its reading range, because of the attendant advantages in resolution and accuracy. Table I illustrates the small scatter of the primary sensor data from the sounder probe. The average deviation of data points from quadratic fits to seven consecutive points was typically 0.3 count, essentially that expected from the digital resolution alone in the absence of sensor imperfections. There were sensors, however, which held a given reading for one or two samples and then jumped two counts, for example, when operating low in their ranges. These were not primary sensor data and do not appear in Table I.

Merging of the temperature data consisted essentially of using T_2 data in the clouds and T_1 data below the clouds. To give some insight into the agreement of the independent tem-

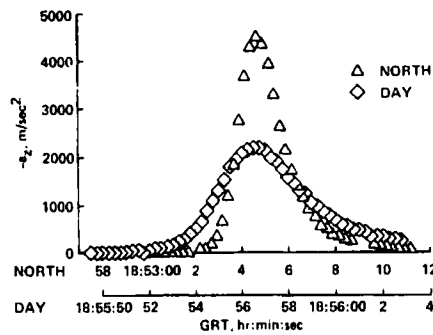


Fig. 3. Deceleration data from the north and day probes. The north probe experienced the largest peak deceleration, 459 g_E , and the shortest pulse, because of the steepness of its flight path, which, at entry into the Venus atmosphere, was inclined 68.7° below horizontal. The day and sounder probe path angles were 25.4° and 32.4° below horizontal, and their peak decelerations were 223 g_E and 277 g_E , respectively.

perature measurements, we show in Figure 5 the differences in the measurements from the T_1 and T_2 sensors. For three of the four probes, the differences were a few tenths K prior to entering the atmosphere, <1 K below 600 K, and <2 K to the end of the measurement period. In the night probe data, differences are <2 K below 560 K, then increase to 3 K at 625 K. The night probe differences exceeded those which we expected, and were due to individual causes, since the difference pattern is not the same for all probes, although it tends to be similar for the day and night probes. Characteristically, however, $T_1 > T_2$ in the small probe data. This we believe is due in part to radiation and conduction errors in T_2 (see below). Conduction of heat down the sensor support post affects T_2 much more than it does T_1 , because the long T_1 sensing wires are self isolating. The sensor support post necessarily passes through the probe boundary layers, which, near the small probes' surfaces, are up to 25 K cooler than the atmosphere during descent [Pitts and Wakefield, this issue]. On the sounder probe, the probe boundary layer where the sensor post is located was heated by the window heater for the solar net flux radiometer windows, which were close to being on the same probe meridian. This may account for $T_2 > T_1$ on the sounder. Sensor radiative emission is greater than absorption and tends to cool T_2 relative to T_1 . This reinforces the temperature difference due to conduction on the small probes. Other possible error sources are in the electronics, where uncertainty in calibration of electronics scale factor could be as large as 0.1%, but is believed to be ~0.05%. The night probe data seem to imply larger scale factor errors, ~0.3%, but we cannot say with assurance how they could occur, especially since electronics scale factors were calibrated intermittently during descent by switching a calibration resistor in place of the sensor resistances. This calibration tested the sum of the independent excitation currents but not the individual currents, so compensating changes in the two current sources could occur and go undetected.

Table 2 lists estimated measurement and electronics errors at 450 and 600 K for the two sensing elements. With the possible exception of T_2 conduction errors, electronics scale factor uncertainty dominates. In the last columns, errors of known sign are combined additively, and their totals are combined root-mean-square with the random scale factor uncertainty. While estimated resultant errors are of the observed magnitude of differences between T_1 and T_2 , they do not fully account for the night probe differences.

The thermal errors of T_1 are all <0.1 K. Because of its greater freedom from radiation and conduction uncertainties, preference was given to use of T_1 data for defining structure of the atmosphere outside of the clouds. Within the clouds, where it was necessary to use T_2 , interpolation indicates that $T_1 - T_2 < 1$ K in all cases, so that there is no important accuracy loss associated with this transition.

Had we used T_2 for defining thermal contrasts in the deep atmosphere, the north-day contrast would have been changed by <1 K; the day-night contrast, by <2 K; and the day-sounder contrast, by <2 K up to 600 K, and by 3 K at 625 K. The largest change would be in the sounder-night contrast, 2.5 K at 500 K, 3.5 K at 600 K, and 4.5 K at 625 K. The sign of this change is to make the night probe profile cooler relative to the sounder profile. It is clearly the night probe profile which is in question, since only its T_1 and T_2 sensors differ by more than 2 K.

It is believed that probe to probe contrasts based on T_1 data are probably accurate within ~1 K and are unlikely to be in error by more than 2 K.

To obtain temperature and pressure of the atmosphere, a correction for probe velocity is made to the measured temperatures and pressures. Thus,

$$p_{\text{atm}} = p_{\text{meas}} - q$$

$$q = \frac{1}{2} \rho V^2$$

$$T_{\text{atm}} = T_{\text{meas}} - \Delta T_{\text{dyn}}$$

$$\Delta T_{\text{dyn}} = \frac{rV^2}{2c_p}$$

(3)

where V is the probe velocity, ρ is atmospheric density, q is dynamic pressure, c_p is the atmospheric specific heat at constant pressure, and r (the recovery factor) is the fraction of the flow kinetic energy resulting in sensor temperature rise (the remaining kinetic energy converted into heat is conducted outward through the sensor boundary layer). The recovery factor was evaluated in preflight laboratory tests and found to be 1.0 within measuring accuracy (± 0.10) at wire diameter Reynolds numbers from 5 to 3000.

At a descent velocity of 40 m/s and for $c_p = 850$ J/kg K (a representative value for CO₂ near 300 K), $\Delta T_{\text{dyn}} = 1$ K. At 10 m/s, $\Delta T_{\text{dyn}} \sim 0.06$ K. The corrections are thus between 1.2 K and 0 in the sounder data after parachute deployment at 65.3 km. Dynamic corrections to the temperature become appreciable at probe velocities of 100 m/s (6 K) to 230 m/s (33 K)

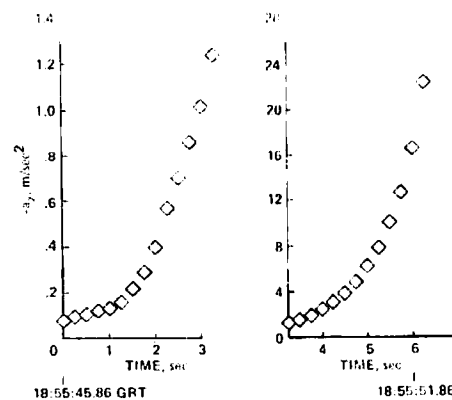


Fig. 4. Day probe accelerations near threshold. The threshold reading of -0.08 m/s² occurs at an altitude of 126 km.

encountered by the small probes early in the descent, at altitudes above 60 km, where uncertainty in probe velocity contributes to uncertainty in T_{atm} . These velocities were carefully determined to within a few percent, so the uncertainty in the correction does not exceed $0.1 \Delta T_{\text{dyn}}$, even in the initial data points. Below 57 km, $\Delta T_{\text{dyn}} < 5$ K in all cases, and the corresponding uncertainty < 0.5 K.

The dynamic pressure correction is nearly constant for probes in equilibrium descent for which, approximately,

$$mg = D = C_D qA$$

or

$$q = \frac{m}{C_D A} g \quad (4)$$

where m and A are the probe mass and frontal area, D is the probe drag force, and C_D is its drag coefficient. This dynamic pressure is typically 22 mbar for the small probes, with a maximum of 30 mbar early in the descent when balance of weight and drag has not been established. The sounder dynamic pressure varied from 33 to 43 mbar in free fall, owing to variations in atmospheric vertical flow velocity and drag coefficient, and was 2 mbar on the parachute. These corrections are essentially negligible or comparable to measurement uncertainty for atmospheric pressures greater than 10 bars, but are important for pressures less than 500 mbar. They are uncertain only to the extent that velocity is uncertain. Thus at $V = 100$ m/s, if $\delta V = 2$ m/s, δq is $0.04 q$ or ~ 1 mbar. Over the bulk of the descent, $\delta q < 0.5$ mbar.

The probe descent velocities were derived from the altitudes by differentiation. The procedure was to fit a marching quadratic to seven consecutive $z(t)$ points and differentiate the quadratic to obtain the vertical component of velocity at point 4. The descent velocities were similar to preflight nominals. The derived velocities were used in computing dynamic corrections to p and T , in an iterative procedure.

ALTITUDE PROFILES OF TEMPERATURE AND PRESSURE BELOW 65 KM

The altitude profiles of temperature and pressure are shown for the four probes in Figures 6 and 7. (Figure 6 includes the data above 65 km from the entry phase of the experiment, to be discussed in the next section.) Below 60 km, the temperature profiles show a mean lapse rate of ~ 8.0 K/km, but there is curvature visible in the profiles within and just below the clouds, and some waviness extending down to 12 km, indicating variable lapse rates. Above 60 km, there is a rapid decrease in lapse rate to ~ 3.5 to 4.0 K/km. This occurs at the altitude of the cloud tops, seen on three of the four probes to lie at 62–64 km [Blamont and Ragent, 1979].

TABLE 1. Results of 7-Point Quadratic Fits to Sounder Pressure Data

Range	Use Range, bars	l count, mbar	Average Residual, mbar	Largest Residual, mbar
A5	23–92	112	27	129
B4	13–23	56	18	61
A4	6.75–12.8	26.8	9	44
B3	3.5–6.7	14.2	5	15
A3	1.8–3.5	7.66	2.4	5.6
B2	0.44–1.8	3.84	0.8	3.0
B1	0.22–0.43	1.01	0.2	0.9

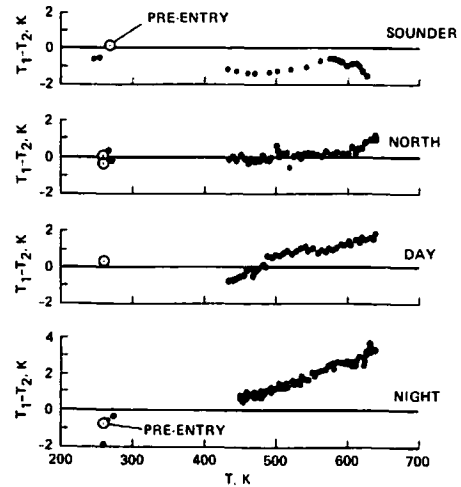


Fig. 5. Temperature differences from the two independent sensors. The T_1 sensor is a fine wire, 0.1 mm diameter, wound around an open supporting frame. The T_2 sensor is a fine wire, 0.025 mm diameter, bonded as a raster onto the leading surface of the outermost member of the support frame. The two sensors use independent excitation current sources, signal amplifiers, and A/D converters. From near the beginning of descent to 430 K, the T_1 sensor data were not valid, due to partial shorting by cloud droplets.

The measured pressure variations with altitude are plotted in Figure 7 with data from the four probes superimposed. The data extend from a minimum of 64 mbar to surface pressures at the four sites ranging from 86.6 to 95.9 bars, reflecting differences in elevation. Terrain elevation differences have been determined by use of the low altitude $p(z)$ data, and altitudes in Figure 7 for all four probes are referenced to the sounder probe landed elevation. Relative to the sounder, the other probes touched down at elevations from +0.98 to -0.65 km. The data then define essentially a single curve for $p(z)$ up to 20 km above which small pressure differences start to appear. The pressure scale height changes by about a factor of 3 between the surface and 60 km, owing to the variation in temperature within the lower atmosphere.

The variations of temperature with pressure from the four probes, shown in Figure 8, have been offset by 20 K from probe to probe for better visibility, since the four sets of data are on top of one another at some levels. There are obvious changes in slope of $T(p)$ at several pressure levels, for example, at 300 mbar, high in the middle cloud, at 1.5 bars, and at 4 bars. Between the latter two levels, there is a highly stable region beneath the clouds [Seiff et al., 1979a, b; Suomi et al., 1979]. (Straight lines have been placed alongside the data to indicate local adiabatic slopes.) Near 1 bar, and just above 10 bars, all four sets of data are approximately adiabatic, but there are three extensive regions of stable lapse rates, one above the clouds, one below the clouds, and for three of the four probes, one in the deep atmosphere near the 40 bar level. (The north probe profile is the exception.)

While data from the four probes are similar, they are not identical. There are, for example, differences in shape of $T(p)$ between 1.5 and 4 bars, where the day and sounder probe data make very gradual transitions, while the night probe data have sharp slope changes. It is also evident that the north probe temperatures are significantly lower than those of the other three probes at pressures below 2 bars, as reported earlier [Seiff et al., 1979a, b].

Tabular data on structure of the lower atmosphere from the four probes are given in Table 3 at altitude intervals of 1 km,

TABLE 2. Estimated Temperature Errors, K

	Radiation		Conduction		Response Lag		Electronics		Root Mean Square	
	450 K	600 K	450 K	600 K	450 K	600 K	450 K	600 K	450 K	600 K
T_1	-0.02	-0.03	0.05	0.04	-0.004	-0.001	0.45	0.6	0.45	0.6
T_2	-0.2	-0.3	<0.64	<0.29	-0.1	-0.03	0.45	0.6	1.1	0.9

for convenience. These data are carefully interpolated from measured values by best fit procedures.

Temperatures were extrapolated graphically below the altitude of sensor breakdown to obtain surface values near 730 K. The extrapolation procedure was iterative. From an initial estimate of $z(t)$, $T(z)$ was extrapolated to obtain a surface temperature, as in Figure 6. This value was plotted with measured surface pressure on the pressure-temperature diagram, Figure 8, to provide an end point to which the $p(T)$ data were smoothly extended, as shown. This $p(T)$ was used in (2) to define second iteration altitudes, and the process was continued to convergence (usually one repetition was sufficient). Surface temperatures obtained this way are probably in doubt by no more than 5 K, and the corresponding altitude uncertainty at 12 km is ~ 40 m. At one point we were using adiabatic extrapolation, with measured pressures, but the departures from adiabatic lapse rate at the 640 K level are sufficient that a clearly visible slope discontinuity was being imposed on $p(T)$. Hence the graphical procedure was judged to be better.

The terrain elevation differences and the associated, sizeable surface pressure differences call attention to the question of the mean surface pressure of the atmosphere of Venus. To determine the mean surface pressure, it is necessary to know the mean planet radius and radii at which measured surface pressures were obtained. This information has not previously

been available. A Pioneer Venus orbiter experiment, the radar altimeter experiment, has determined the mean radius to be 6051.39 km, based on observations of 80% of the planet surface [Pettengill *et al.*, this issue]. Radii in the vicinity of the landing sites of the three small probes have also been determined. Table 4 (G. Pettengill, private communication, 1979). In the third column, terrain elevation is given relative to the day probe from these measurements and is compared with that given by the pressure data in column 4. The measurements agree, well within the indicated uncertainty.

On the basis of a careful study of terrain contours near the north probe landing site provided by H. Mazursky (private communication, 1979) we have adopted a value of $R_0 = 6053.0 \pm 0.25$ km for that site. From this, and the terrain elevations of the other probes indicated by the pressure data, we have made the following table of landed radii and pressures (Table 5).

The absolute uncertainty in landed radius is, for each probe, ± 0.25 km, derived from the north probe radius uncertainty. The relative uncertainty from probe to probe is smaller, ~ 0.1 km, corresponding to pressure errors of 0.6%. We have given the radii for the day, night, and sounder probes to the nearest 0.01 km corresponding to a north probe radius of exactly 6053.00 km and pressure data accurate within 0.1%. At the mean radius, we assign a pressure of 95.7

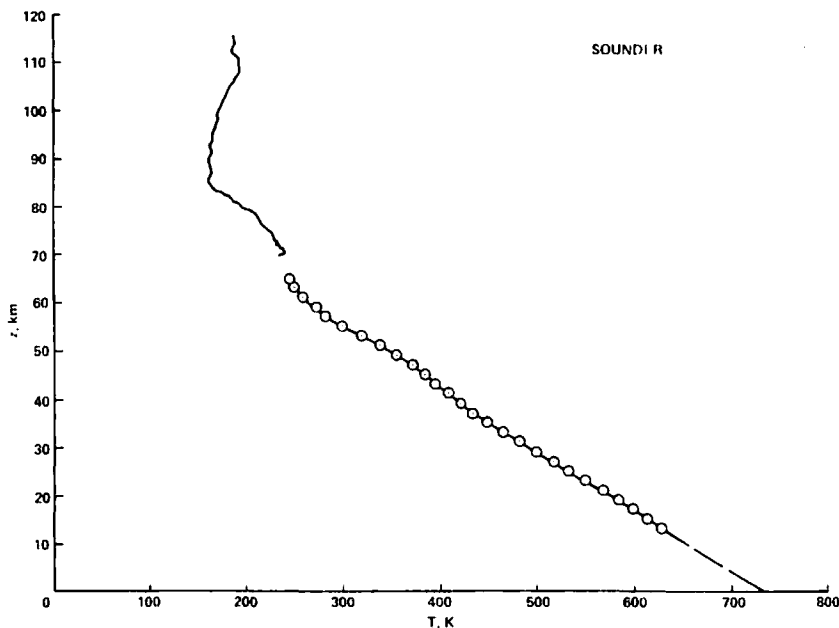


Fig. 6a

Fig. 6. Temperature soundings obtained during entry of the four Pioneer Venus probes: (a) sounder; (b) day probe; (c) north probe; (d) night probe. Altitudes are measured above the individual landing sites. The data below about 65 km, shown by symbols, were the result of direct sensing of temperature and pressure. The data above 65 km were derived from measurements of atmospheric densities defined by probe decelerations during high speed entry into the atmosphere. The latter data have not been analyzed for the night probe. Curvature in the profiles (i.e., variability in lapse rate) is visible between 60 and 40 km, and to a lesser degree, all the way to the surface. Waves in the temperature profiles are present above ~ 90 km, increasing in amplitude with height.

± 1.4 bars. The primary uncertainty is that associated with the probe landing site radii. One of the four Pioneer Venus probes landed near the mean radius, while the other three landed above it. It may be possible to update and improve the information on landed radii and pressure at the mean surface as further analysis of the radar elevation data becomes available.

ATMOSPHERE STRUCTURE FROM 65 TO 125 KM

Atmospheric densities in the altitude range above 65 km were derived from probe deceleration measurements during the period of high-speed entry into the atmosphere at an initial velocity of 11.5 km/s. The aerodynamic drag force D which decelerates the probe is proportional to the ambient atmospheric density ρ and the square of the flight velocity V . The governing equation is

$$D = -ma = C_D \frac{1}{2} \rho V^2 A \tag{5}$$

where m is the probe mass and a is the deceleration, C_D is the drag coefficient, and A is probe frontal area. We solve for the density,

$$\rho = -2 \frac{m}{C_D A} \frac{a}{V^2} \tag{6}$$

The vehicle parameters, mass and frontal area, are known at entry into the atmosphere from preflight measurements. The mass loss and area change resulting from ablation during entry were small (~ 3 and 1.4%, respectively) and were estimated as a function of time for each probe individually by the heat shield contractor and provided to us by the Pioneer Project Office. The drag coefficient was accurately established by tests in air and in CO₂ of small models of the probes at conditions simulating those of the Venus entries by our colleague, Peter Intrieri. The models were launched from light gas guns at speeds up to 5 km/s into a ballistic range, the Ames Hypervelocity Free Flight Facility, where their decelerations were measured and reduced to drag coefficients by use of (5). Some of the data obtained are reproduced in Figure 9 (P. F. Intrieri, private communication, 1978), where the variation in C_D with Mach number at Reynolds numbers $> 0.5 \times 10^6$ and the variation with Reynolds number at a flight velocity of 4.6 km/s are shown. At hypersonic speeds, the drag coefficient ap-

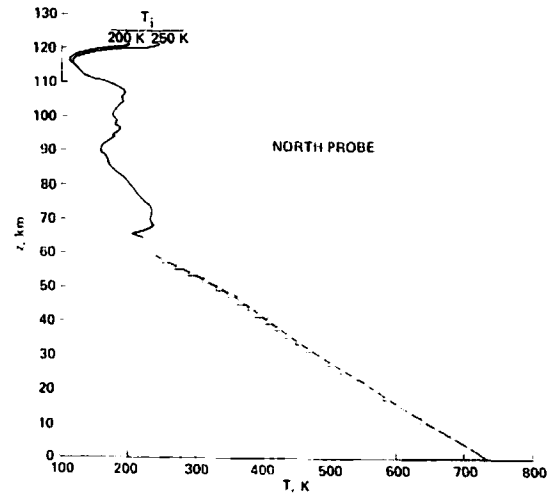


Fig. 6c

proaches a constant value of 1.05 at high Reynolds numbers; and the variation with Reynolds number is small down to $Re = 10^3$, where viscous and slip flow effects start to become significant. These curves were used to select $C_D(t)$ on the basis of flight Mach and Reynolds numbers.

The velocity in (6) is computed from measured decelerations and the velocity at entry into the atmosphere, known from tracking the probes in space to within ~0.1 m/s, Table 6. The four probes differed appreciably in flight path angle (below horizontal), the north probe entering most steeply, and the day probe most obliquely. The four entries were simultaneous within ~10 min. The procedures for velocity and flight path angle reconstruction during entry have been more fully described in earlier publications [Seiff and Kirk, 1977; Seiff et al., 1973].

For the Pioneer Venus configuration the effect of probe angles of attack on C_D is very moderate (e.g., at 20° angle of attack, <2% in continuum flow and <9% at $Re = 500$). If the probes crossed the 200-km level with the nominal angles of attack given us by the Pioneer Venus Project Office (J. R. Cowley, private communication, 1978), namely 0.1°, 18°, 20°, and 12°, for the sounder, north, night, and day probes, respectively, then the increasing dynamic pressure during entry would cause convergence to <1° amplitude during the measurement interval. At this amplitude, angle of attack would have no detectable effect on the measurements.

Equation 6 is used to determine $\rho(t)$. Probe altitude as a function of time, $z(t)$, is determined by integration of the measured accelerations in the equations of motion [Seiff and Kirk, 1977], given the velocity V_E and flight path angle below hori-

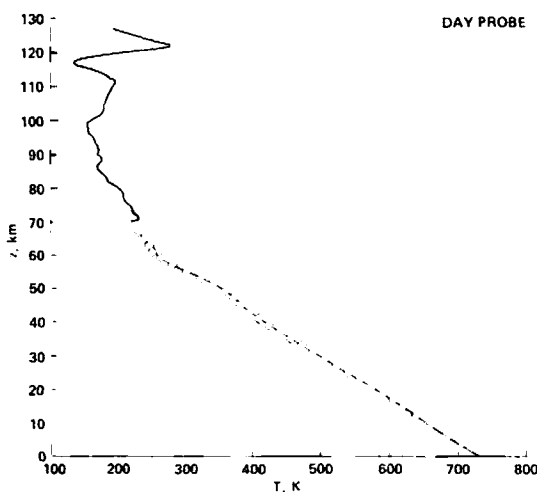


Fig. 6b

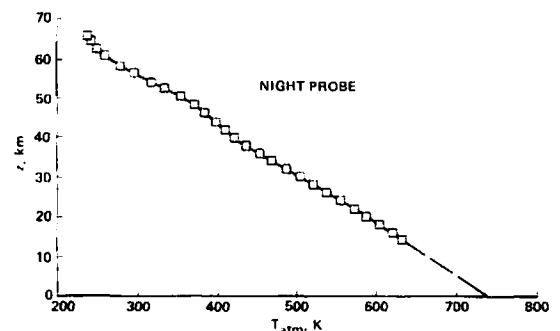


Fig. 6d

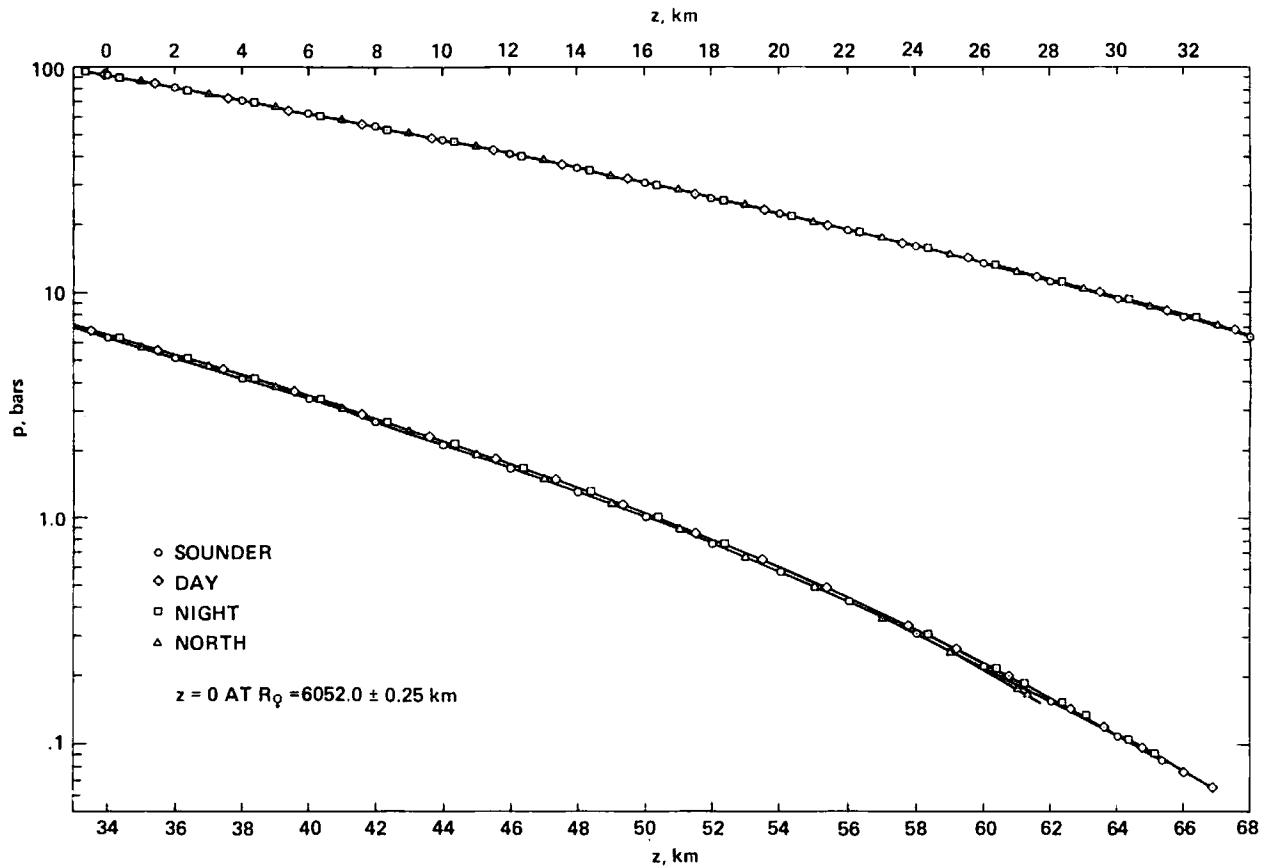


Fig. 7. Pressure profiles in the lower atmosphere of Venus from the four Pioneer Venus probes. Altitudes are referenced to the sounder probe landing site. The four probes define essentially a single profile up to 20 km, then start to diverge and indicate small pressure differences. These differences are smaller in the current analysis than in the preliminary analysis [Seiff *et al.*, 1979b].

zonal γ_E at 200 km. Table 6. The altitude $z(t)$ is thus defined relative to an arbitrarily selected reference level of 200 km, well above the region of detectable aerodynamic force. Since the entry phase was terminated at the time of the probe descent mode command (at 60 to 66 km), a second reference altitude, the altitude at mode change, was available to check the altitude determination. Altitude at mode change is known from the descent mode data as described in the preceding section.

Velocity also was required to be continuous at mode change. Accuracy of the entry mode velocity at mode change was limited to, at best, ~ 10 m/s by uncertainty in knowledge of the instrument electronics scale factor on 600 g_E range. Hence this scale factor was adjusted to obtain an accurate match to the velocity from descent mode data, at mode change. This adjustment was important for preserving accuracy in the density data near the end of the entry period.

Given $\rho(z)$, the equation of hydrostatic equilibrium (1) was integrated to define $p(z)$; and the equation of state was used to define $T(z)$. This required that the molecular weight profile $\mu(z)$ be specified.

The molecular weight adopted for the lower atmosphere was 43.44, which corresponds to an atmosphere with 0.965 mole fraction of CO_2 , 0.035 N_2 , 180 ppm SO_2 , 60 ppm Ar, and 30 ppm CO [Oyama *et al.*, 1980; Hoffman *et al.*, 1980]. (This differs by 0.6% from the value, 43.7, used in our preliminary analysis.) In the upper atmosphere, because of photodissocia-

tion, etc., the molecular weight decreases. At 130 km, the model fit to the data of Bus neutral mass spectrometer indicates $\mu = 39.8$ [von Zahn *et al.*, this issue], while an extrapolation of the dayside data of the Orbiter neutral mass spectrometer [Niemann *et al.*, 1979, this issue] indicates $\mu = 41$. Extrapolation to 130 km of the dayside atmospheric model developed from the orbiter drag experiment [Keating *et al.*, 1979a, b, 1980] also indicates $\mu = 41$. At 95 km, earth-based microwave measurements have indicated the CO mole fraction is 10^{-4} [Muhleman *et al.*, 1979; Wilson and Klein, 1979], that is, the CO photodissociated from CO_2 in the upper atmosphere is essentially recombined, and we assume small departure from the lower atmospheric $\mu = 43.44$. Above 130 km, μ decreases rapidly, as the O and CO fractions increase [von Zahn *et al.*, this issue]. At the time of the analysis, on the basis of all these data, we selected the following table (Table 7) to describe $\mu(z)$ for altitudes above 80 km. These values plot on a smooth curve extending from the lower atmospheric value at 80 km with minimal photodissociation below 100 km to a value near those of the orbiter NMS and orbiter atmospheric drag experiment extrapolations.

The selected variation probably represents the upper limit of μ at the higher altitudes. The values interpolated graphically between the lower atmospheric value and the BNMS model value at 130 km are also shown for comparison. Had they been used instead, temperatures would be lowered by 2.9% (5.7 K) at 125 km, 1.7% (3.3 K) at 120 km, and 0.5% (1

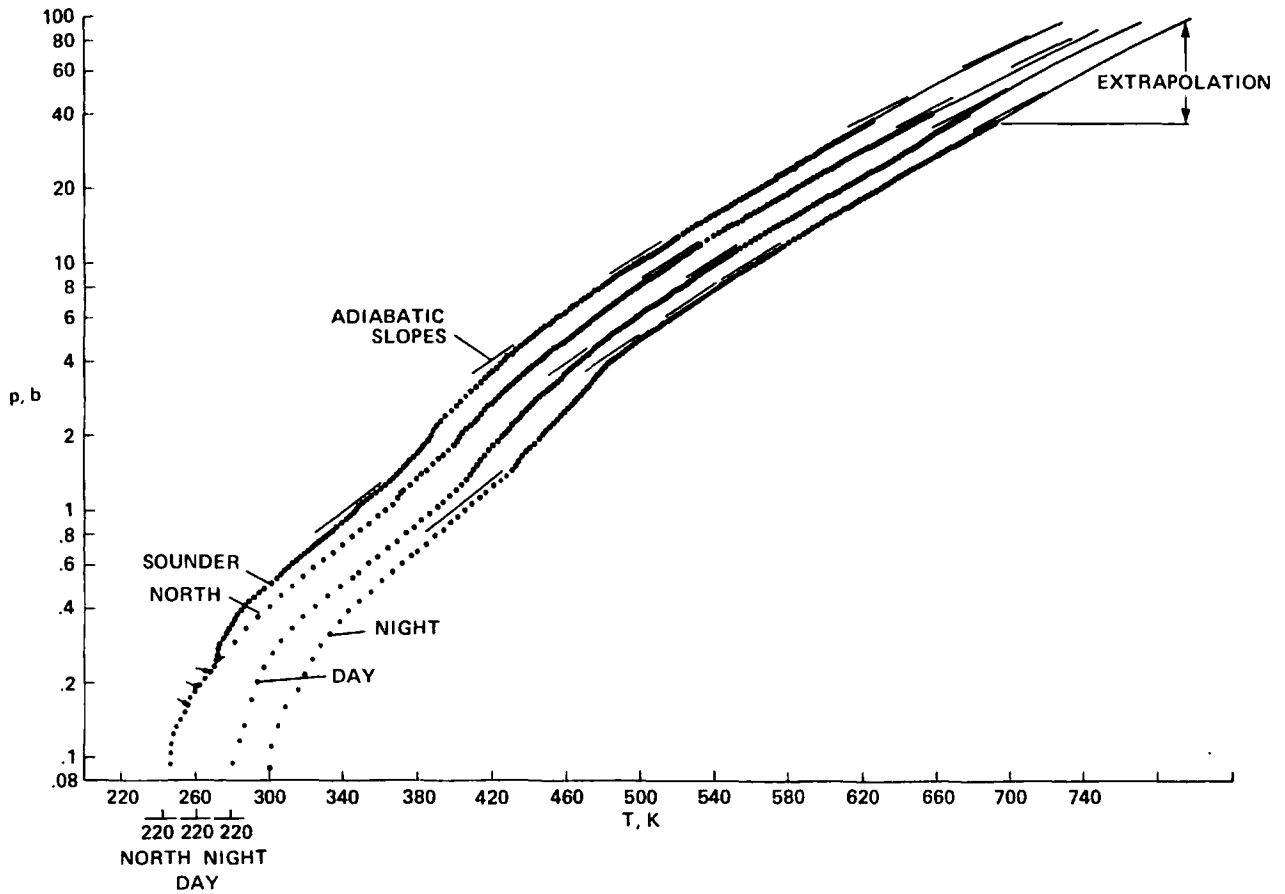


Fig. 8. Temperature as a function of pressure from the four probes. The data plotted are the complete set of merged data from the small probes. For the sounder, above every second or third point is plotted depending on altitude. The data have been offset 20 K from probe to probe to improve readability. The straight lines indicate local adiabatic slopes. The four flagged symbols are north probe data in a region of overlap with the sounder data.

K) at 110 km. Refinement of these choices, with day/night distinctions, will probably become possible as the upper atmospheric data are further analyzed.

Temperatures, densities, and pressures derived from the deceleration data by use of the above procedures are shown in Figures 6, 10, and 11 for three of the four probes. The temperature lapse rate of 3.5–4 K/km above the clouds is a stable lapse rate. Hence it would seem appropriate to designate this as the principal Venus stratosphere, although it will be noted that there are two lower stable layers, one of appreciable depth. The main stratospheric base is at the 100 to 200 mbar level, in common with the stratospheres of earth (*U.S. Standard Atmosphere*, 1962), and of Jupiter [*Hanel et al.*, 1979]. Above 85–90 km, the atmosphere is essentially isothermal up to 110 km, except for small amplitude waviness. (Note that T oscillations of vertical height less than the altitude resolution, e.g., 2.7 km on the north probe at 95 km, are to be regarded as measurement noise, probably introduced in data processing or smoothing. Waves with $\lambda > 7.5$ km are probably real.) In the case of the day and north probes, the oscillation amplitude grows rapidly above 110 km and dominates the profile. Wave amplitude increases with height to ~ 75 K at 120 km, with vertical wavelengths ~ 15 or 20 km. Two initial temperatures were assumed for each probe and are shown in the case of the north probe. The resulting wave profiles converge rapidly and are indistinguishable below 115 km. Waves similar to these

were seen in the upper atmosphere of Mars [*Seiff and Kirk*, 1977; *Nier et al.*, 1977], and are a result of oscillatory motions with a vertical component, perhaps atmospheric thermal tides.

Just above the clouds, a temperature inversion is observed in the north probe data, and to a degree which diminishes with latitude in the other profiles as well. The north probe inversion layer is 2.5 km deep, with a lapse rate of +12.8 K/km. Similar inversions have been seen persistently in radio occultation profiles [*Howard et al.*, 1974; *Kliore and Patel*, this issue], with which we shall make detailed comparisons, and again, with smaller amplitudes ~ 4 K near the equator. We suggest that this inversion characterizes the region of temperature adjustment between the upper clouds and the stratosphere. Both regions may be in radiative equilibrium, but equilibrium temperatures differ because of particle content.

An altitude gap of a few km is left in the temperature data near the lower end of the entry period. This is the region where atmospheric winds become sizeable relative to probe velocity, and must be included vectorially in (6). Hence, unless the winds are well determined, temperature can be in significant error. Consequently there is some possibility (which we have not had time to fully explore) of inferring the winds from the requirement on continuity of $\rho(z)$ and $p(z)$. The temperature data are terminated where probe velocity = 1 km/s, at which wind effects would not seriously alter the data.

Density data measured during entry and descent are shown

TABLE 3a. Lower Atmosphere State Properties: Sounder Probe

Altitude, km	p , bars	T , K	ρ , kg/m ³	GRT	GRT, s
64.83	0.925 - 01	246.3	0.1964E + 00	1849.646	67778.8
64.00	0.1078E + 00	247.0	0.2282E + 00	1849.995	67799.7
63.00	0.1294E + 00	249.3	0.2716E + 00	1850.447	67826.8
62.00	0.1551E + 00	254.8	0.3183E + 00	1850.944	67856.6
61.00	0.1851E + 00	259.7	0.3728E + 00	1851.470	67888.2
60.00	0.2199E + 00	268.1	0.4291E + 00	1852.059	67923.5
59.00	0.2602E + 00	272.0	0.5004E + 00	1852.672	67960.3
58.00	0.3073E + 00	276.0	0.5825E + 00	1853.333	68000.0
57.00	0.3618E + 00	281.3	0.6732E + 00	1854.052	68043.1
56.00	0.4247E + 00	288.9	0.7694E + 00	1854.819	68089.1
55.00	0.4959E + 00	299.4	0.8671E + 00	1855.643	68138.6
54.00	0.5760E + 00	309.5	0.9745E + 00	1856.522	68191.3
53.00	0.6659E + 00	319.8	0.1091E + 01	1857.478	68248.7
52.00	0.7665E + 00	329.5	0.1219E + 01	1858.442	68306.5
51.00	0.8788E + 00	338.7	0.1360E + 01	1859.481	68368.8
50.00	0.1004E + 01	347.3	0.1515E + 01	1900.568	68434.1
49.00	0.1144E + 01	355.3	0.1688E + 01	1901.716	68503.0
48.00	0.1299E + 01	364.9	0.1867E + 01	1902.944	68576.6
47.00	0.1471E + 01	371.8	0.2075E + 01	1904.207	68652.4
46.00	0.1662E + 01	379.4	0.2298E + 01	1905.533	68732.0
45.00	0.1874E + 01	384.4	0.2558E + 01	1906.527	68791.6
44.00	0.2109E + 01	389.4	0.2843E + 01	1906.862	68811.7
43.00	0.2371E + 01	394.8	0.3153E + 01	1907.177	68830.6
42.00	0.2661E + 01	401.4	0.3482E + 01	1907.514	68850.8
41.00	0.2981E + 01	407.9	0.3839E + 01	1907.865	68871.9
40.00	0.3334E + 01	414.7	0.4223E + 01	1908.235	68894.1
39.00	0.3722E + 01	421.6	0.4638E + 01	1908.632	68917.9
38.00	0.4147E + 01	428.1	0.5092E + 01	1909.046	68942.8
37.00	0.4615E + 01	435.1	0.5575E + 01	1909.479	68968.8
36.00	0.5125E + 01	443.0	0.6082E + 01	1909.931	68995.9
35.00	0.5682E + 01	450.3	0.6636E + 01	1910.400	69024.0
34.00	0.6289E + 01	458.4	0.7217E + 01	1910.894	69053.6
33.00	0.6950E + 01	466.3	0.7841E + 01	1911.376	69082.6
32.00	0.7666E + 01	474.6	0.8500E + 01	1911.901	69114.1
31.00	0.8443E + 01	482.9	0.9200E + 01	1912.457	69147.4
30.00	0.9283E + 01	491.8	0.9935E + 01	1913.053	69183.2
29.00	0.1019E + 02	500.5	0.1072E + 02	1913.667	69220.0
28.00	0.1117E + 02	508.8	0.1155E + 02	1914.299	69257.9
27.00	0.1222E + 02	517.1	0.1244E + 02	1914.921	69295.3
26.00	0.1336E + 02	524.9	0.1340E + 02	1915.543	69332.6
25.00	0.1458E + 02	533.7	0.1438E + 02	1916.251	69375.0
24.00	0.1589E + 02	542.2	0.1543E + 02	1916.981	69418.9
23.00	0.1730E + 02	550.5	0.1654E + 02	1917.721	69463.3
22.00	0.1880E + 02	558.7	0.1771E + 02	1918.503	69510.2
21.00	0.2042E + 02	567.0	0.1895E + 02	1919.303	69558.2
20.00	0.2214E + 02	575.5	0.2025E + 02	1920.142	69608.5
19.00	0.2399E + 02	583.7	0.2162E + 02	1921.034	69662.0
18.00	0.2596E + 02	590.6	0.2312E + 02	1921.782	69706.9
17.00	0.2806E + 02	598.7	0.2466E + 02	1922.707	69762.4
16.00	0.3031E + 02	606.1	0.2629E + 02	1923.665	69819.9
15.00	0.3271E + 02	613.9	0.2799E + 02	1924.653	69879.2
14.00	0.3526E + 02	620.9	0.2982E + 02	1925.629	69937.7
13.00	0.3797E + 02	627.8	0.3175E + 02	1926.605	69996.3
12.00	0.4086E + 02	636.0	0.3371E + 02	1927.663	70059.8
11.00	0.4394E + 02	642.6	0.3586E + 02	1928.745	70124.7
10.00	0.4720E + 02	651.3	0.3798E + 02	1929.858	70191.5
9.00	0.5066E + 02	658.5	0.4028E + 02	1931.003	70260.2
8.00	0.5432E + 02	666.6	0.4262E + 02	1932.198	70331.9
7.00	0.5820E + 02	673.9	0.4514E + 02	1933.446	70406.7
6.00	0.6231E + 02	681.9	0.4770E + 02	1934.705	70482.3
5.00	0.6665E + 02	690.1	0.5037E + 02	1935.994	70559.7
4.00	0.7123E + 02	698.4	0.5314E + 02	1937.307	70638.4
3.00	0.7606E + 02	706.3	0.5602E + 02	1938.682	70720.9
2.00	0.8115E + 02	715.1	0.5893E + 02	1940.105	70806.3
1.00	0.8652E + 02	722.7	0.6208E + 02	1941.579	70894.8
0.00	0.9216E + 02	730.9	0.6528E + 02	1943.117	70987.0

Altitudes are relative to the sounder probe landing site. $R_0 = 6052.0$ km, $g_0 = 8.8694$ m/s², $\mu = 43.44$.
GRT 1849.646 = 18 hours, 49.646 minutes.

TABLE 3b. Lower Atmosphere State Properties: Day Probe

Altitude, km	p , bars	T , K	ρ , kg/m ³	GRT	GRT, s
66.85	0.6407E - 01	233.2	0.1436E + 00	1856.324	68179.4
66.00	0.7551E - 01	236.1	0.1673E + 00	1856.457	68187.4
65.00	0.9130E - 01	239.4	0.1995E + 00	1856.563	68193.8
64.00	0.1102E + 01	242.8	0.2374E + 00	1856.675	68200.5
63.00	0.1328E + 00	246.2	0.2820E + 00	1856.803	68208.2
62.00	0.1595E + 00	249.4	0.3345E + 00	1856.937	68216.2
61.00	0.1912E + 00	252.8	0.3955E + 00	1857.082	68224.9
60.00	0.2285E + 00	257.6	0.4641E + 00	1857.250	68235.0
59.00	0.2722E + 00	263.9	0.5395E + 00	1857.429	68245.8
58.00	0.3227E + 00	271.1	0.6228E + 00	1857.611	68256.6
57.00	0.3806E + 00	280.9	0.7091E + 00	1857.833	68270.0
56.00	0.4464E + 00	291.3	0.8022E + 00	1858.039	68282.4
55.00	0.5203E + 00	302.6	0.9004E + 00	1858.268	68296.1
54.00	0.6034E + 00	313.9	0.1007E + 01	1858.512	68310.7
53.00	0.6963E + 00	323.9	0.1126E + 01	1858.774	68326.4
52.00	0.8000E + 00	334.4	0.1254E + 01	1859.053	68343.2
51.00	0.9156E + 00	343.2	0.1398E + 01	1859.348	68360.9
50.00	0.1044E + 01	351.7	0.1557E + 01	1859.630	68377.8
49.00	0.1188E + 01	360.5	0.1727E + 01	1859.956	68397.4
48.00	0.1347E + 01	366.8	0.1926E + 01	1900.288	68417.3
47.00	0.1525E + 01	372.3	0.2148E + 01	1900.660	68439.6
46.00	0.1723E + 01	377.9	0.2392E + 01	1901.013	68460.8
45.00	0.1943E + 01	384.7	0.2650E + 01	1901.398	68483.9
44.00	0.2187E + 01	390.7	0.2938E + 01	1901.826	68509.6
43.00	0.2457E + 01	396.6	0.3253E + 01	1902.269	68536.1
42.00	0.2756E + 01	402.9	0.3593E + 01	1902.730	68563.8
41.00	0.3086E + 01	410.1	0.3953E + 01	1903.217	68593.0
40.00	0.3449E + 01	417.2	0.4343E + 01	1903.737	68624.2
39.00	0.3847E + 01	424.7	0.4761E + 01	1904.292	68657.5
38.00	0.4283E + 01	432.3	0.5208E + 01	1904.866	68691.9
37.00	0.4760E + 01	439.9	0.5689E + 01	1905.459	68727.6
36.00	0.5281E + 01	448.1	0.6198E + 01	1906.069	68764.1
35.00	0.5849E + 01	455.7	0.6751E + 01	1906.692	68801.5
34.00	0.6466E + 01	463.6	0.7336E + 01	1907.362	68841.7
33.00	0.7136E + 01	472.6	0.7943E + 01	1908.072	68884.3
32.00	0.7862E + 01	480.7	0.8607E + 01	1908.784	68927.0
31.00	0.8647E + 01	489.1	0.9305E + 01	1909.560	68973.6
30.00	0.9497E + 01	497.6	0.1005E + 02	1910.352	69021.1
29.00	0.1041E + 02	506.3	0.1083E + 02	1911.177	69070.6
28.00	0.1140E + 02	514.6	0.1166E + 02	1911.983	69119.0
27.00	0.1246E + 02	523.2	0.1254E + 02	1912.863	69171.8
26.00	0.1361E + 02	532.1	0.1346E + 02	1913.780	69226.8
25.00	0.1483E + 02	540.2	0.1446E + 02	1914.731	69283.8
24.00	0.1615E + 02	548.4	0.1550E + 02	1915.674	69340.5
23.00	0.1756E + 02	557.6	0.1658E + 02	1916.748	69404.9
22.00	0.1907E + 02	566.5	0.1772E + 02	1917.864	69471.9
21.00	0.2069E + 02	574.7	0.1894E + 02	1918.973	69538.4
20.00	0.2241E + 02	582.5	0.2024E + 02	1920.080	69604.8
19.00	0.2425E + 02	591.3	0.2158E + 02	1921.291	69677.4
18.00	0.2622E + 02	599.0	0.2302E + 02	1922.473	69748.4
17.00	0.2832E + 02	606.6	0.2454E + 02	1923.631	69817.9
16.00	0.3055E + 02	613.8	0.2615E + 02	1924.825	69889.5
15.00	0.3293E + 02	620.7	0.2787E + 02	1925.987	69959.2
14.00	0.3547E + 02	627.9	0.2966E + 02	1927.242	70034.5
13.00	0.3817E + 02	634.7	0.3156E + 02	1928.527	70111.6
12.00	0.4105E + 02	641.9	0.3354E + 02	1929.854	70191.2
11.00	0.4410E + 02	649.5	0.3559E + 02	1931.199	70271.9
10.00	0.4734E + 02	656.3	0.3778E + 02	1932.672	70360.3
9.00	0.5078E + 02	663.8	0.4003E + 02	1934.274	70456.4
8.00	0.5442E + 02	671.0	0.4240E + 02	1936.210	70572.6
7.00	0.5828E + 02	678.2	0.4489E + 02	1937.987	70679.2
6.00	0.6237E + 02	686.0	0.4744E + 02	1939.572	70774.3
5.00	0.6669E + 02	693.4	0.5014E + 02	1941.280	70876.8
4.00	0.7125E + 02	701.0	0.5294E + 02	1943.091	70985.5
3.00	0.7606E + 02	709.0	0.5578E + 02	1944.990	71099.4
2.00	0.8113E + 02	717.0	0.5875E + 02	1946.934	71216.1
1.00	0.8648E + 02	724.7	0.6185E + 02	1948.925	71335.5
0.00	0.9210E + 02	732.4	0.6509E + 02	1950.997	71459.8
-0.10	0.9268E + 02	733.0	0.6544E + 02	1951.183	71471.0

Altitudes are relative to the sounder probe landing site at 6052.0 km. $R_0 = 6051.9$ km, $g_0 = 8.8697$ m/s², $\mu = 43.44$. GRT 1856.324 = 18 hours, 56.324 minutes.

TABLE 3c. Lower Atmosphere State Properties: Night Probe

Altitude, km	p , bars	T , K	ρ , kg/m ³	GRT	GRT, s
65.13	0.9046E - 01	238.3	0.1985E + 00	1859.820	68389.2
65.00	0.9279E - 01	238.5	0.2034E + 00	1859.836	68390.2
64.00	0.1121E + 00	241.3	0.2430E + 00	1859.960	68397.6
63.00	0.1350E + 00	245.9	0.2872E + 00	1900.096	68405.7
62.00	0.1621E + 00	251.1	0.3378E + 00	1900.234	68414.1
61.00	0.1939E + 00	257.7	0.3935E + 00	1900.384	68423.0
60.00	0.2310E + 00	261.9	0.4614E + 00	1900.545	68432.7
59.00	0.2744E + 00	267.5	0.5366E + 00	1900.719	68443.1
58.00	0.3245E + 00	274.8	0.6179E + 00	1900.917	68455.0
57.00	0.3823E + 00	281.6	0.7105E + 00	1901.116	68467.0
56.00	0.4482E + 00	291.8	0.8040E + 00	1901.336	68480.2
55.00	0.5226E + 00	301.7	0.9067E + 00	1901.564	68493.9
54.00	0.6065E + 00	311.6	0.1019E + 01	1901.805	68508.3
53.00	0.7005E + 00	332.1	0.1139E + 01	1902.071	68524.3
52.00	0.8054E + 00	322.0	0.1271E + 01	1902.347	68540.8
51.00	0.9227E + 00	340.2	0.1421E + 01	1902.629	68557.7
50.00	0.1054E + 01	348.7	0.1584E + 01	1902.932	68575.9
49.00	0.1199E + 01	357.8	0.1758E + 01	1903.251	68595.1
48.00	0.1361E + 01	366.9	0.1945E + 01	1903.586	68615.1
47.00	0.1540E + 01	373.4	0.2164E + 01	1903.947	68636.8
46.00	0.1739E + 01	379.1	0.2407E + 01	1904.330	68659.8
45.00	0.1961E + 01	386.1	0.2665E + 01	1904.730	68683.8
44.00	0.2206E + 01	392.3	0.2952E + 01	1905.159	68709.5
43.00	0.2478E + 01	398.6	0.3264E + 01	1905.606	68736.3
42.00	0.2778E + 01	404.8	0.3604E + 01	1906.063	68763.8
41.00	0.3109E + 01	410.9	0.3975E + 01	1906.554	68793.2
40.00	0.3474E + 01	416.7	0.4380E + 01	1907.050	68823.0
39.00	0.3877E + 01	422.2	0.4825E + 01	1907.577	68854.6
38.00	0.4319E + 01	430.9	0.5268E + 01	1908.152	68889.1
37.00	0.4801E + 01	438.8	0.5752E + 01	1908.725	68923.5
36.00	0.5327E + 01	448.0	0.6253E + 01	1909.352	68961.1
35.00	0.5899E + 01	456.2	0.6802E + 01	1909.984	68999.0
34.00	0.6521E + 01	464.1	0.7391E + 01	1910.606	69036.4
33.00	0.7196E + 01	473.1	0.8003E + 01	1911.326	69079.6
32.00	0.7927E + 01	481.5	0.8663E + 01	1912.032	69121.9
31.00	0.8717E + 01	490.2	0.9360E + 01	1912.797	69167.8
30.00	0.9571E + 01	499.0	0.1010E + 02	1913.597	69215.8
29.00	0.1049E + 02	507.6	0.1088E + 02	1914.403	69264.2
28.00	0.1149E + 02	516.0	0.1172E + 02	1915.248	69314.9
27.00	0.1255E + 02	524.9	0.1259E + 02	1916.142	69368.5
26.00	0.1370E + 02	533.0	0.1353E + 02	1917.015	69420.9
25.00	0.1493E + 02	541.6	0.1452E + 02	1917.951	69477.1
24.00	0.1626E + 02	550.1	0.1556E + 02	1918.925	69535.5
23.00	0.1767E + 02	558.5	0.1666E + 02	1919.918	69595.1
22.00	0.1919E + 02	566.8	0.1782E + 02	1920.924	69655.4
21.00	0.2081E + 02	574.6	0.1906E + 02	1921.958	69717.5
20.00	0.2255E + 02	582.8	0.2036E + 02	1923.043	69782.6
19.00	0.2440E + 02	591.0	0.2172E + 02	1924.193	69851.6
18.00	0.2638E + 02	599.3	0.2315E + 02	1925.440	69926.4
17.00	0.2849E + 02	607.4	0.2465E + 02	1926.706	70002.3
16.00	0.3073E + 02	616.5	0.2619E + 02	1928.077	70084.6
15.00	0.3311E + 02	624.0	0.2786E + 02	1929.372	70162.3
14.00	0.3565E + 02	631.4	0.2963E + 02	1930.681	70240.9
13.00	0.3835E + 02	639.6	0.3145E + 02	1932.073	70324.4
12.00	0.4121E + 02	646.8	0.3340E + 02	1933.402	70404.1
11.00	0.4425E + 02	654.1	0.3544E + 02	1934.888	70493.3
10.00	0.4748E + 02	660.8	0.3761E + 02	1936.424	70585.4
9.00	0.5090E + 02	668.8	0.3979E + 02	1937.930	70675.8
8.00	0.5452E + 02	676.5	0.4211E + 02	1939.484	70769.1
7.00	0.5836E + 02	682.9	0.4461E + 02	1941.099	70865.9
6.00	0.6242E + 02	689.8	0.4720E + 02	1942.755	70965.3
5.00	0.6671E + 02	697.0	0.4988E + 02	1944.469	71068.1
4.00	0.7125E + 02	704.6	0.5263E + 02	1946.251	71175.0
3.00	0.7604E + 02	711.6	0.5554E + 02	1948.082	71284.9
2.00	0.8109E + 02	719.1	0.5852E + 02	1950.018	71401.1
1.00	0.8642E + 02	726.3	0.6166E + 02	1952.009	71520.5
0.00	0.9203E + 02	733.8	0.6489E + 02	1954.037	71642.2
-0.65	0.9583E + 02	738.5	0.6708E + 02	1955.317	71719.0

Altitudes are relative to the sounder probe landing site at 6052.0 km. $R_0 = 6051.4$ km, $g_0 = 8.8712$ m/s², $\mu = 43.44$. GRT 1859.820 = 18 hours, 59.820 minutes.

TABLE 3d. Lower Atmosphere State Properties: Night Probe

Altitude, km	p , bars	T , K	ρ , kg/m ³	GRT	GRT, s
61.28	0.1650E + 00	234.0	0.3687E + 00	1853.405	68004.3
61.00	0.1739E + 00	236.3	0.3850E + 00	1353.447	68006.8
60.00	0.2103E + 00	243.1	0.4522E + 00	1853.600	68016.0
59.00	0.2528E + 00	251.2	0.5263E + 00	1853.776	68026.6
58.00	0.3018E + 00	262.4	0.6018E + 00	1853.963	68037.8
57.00	0.3580E + 00	271.6	0.6897E + 00	1854.158	68049.5
56.00	0.4220E + 00	282.2	0.7826E + 00	1854.379	68062.8
55.00	0.4946E + 00	292.6	0.8846E + 00	1854.617	68077.0
54.00	0.5765E + 00	303.2	0.9954E + 00	1854.856	68091.4
53.00	0.6685E + 00	313.7	0.1116E + 01	1855.118	68107.1
52.00	0.7715E + 00	323.7	0.1248E + 01	1855.376	68122.6
51.00	0.8865E + 00	334.0	0.1391E + 01	1855.666	68139.9
50.00	0.1014E + 01	344.1	0.1545E + 01	1855.972	68158.3
49.00	0.1157E + 01	350.3	0.1731E + 01	1856.273	68176.4
48.00	0.1316E + 01	358.8	0.1924E + 01	1856.631	68197.9
47.00	0.1494E + 01	367.0	0.2134E + 01	1856.991	68219.5
46.00	0.1690E + 01	375.0	0.2364E + 01	1857.361	68241.7
45.00	0.1907E + 01	382.0	0.2620E + 01	1857.758	68265.5
44.00	0.2149E + 01	387.6	0.2910E + 01	1858.178	68290.7
43.00	0.2417E + 01	393.3	0.3226E + 01	1858.619	68317.2
42.00	0.2714E + 01	400.2	0.3561E + 01	1859.073	68344.4
41.00	0.3041E + 01	407.2	0.3922E + 01	1859.564	68373.9
40.00	0.3401E + 01	414.5	0.4311E + 01	1900.077	68404.6
39.00	0.3797E + 01	421.7	0.4731E + 01	1900.609	68436.5
38.00	0.4230E + 01	429.3	0.5179E + 01	1901.151	68469.1
37.00	0.4705E + 01	437.3	0.5656E + 01	1901.742	68504.5
36.00	0.5223E + 01	445.3	0.6167E + 01	1902.341	68540.4
35.00	0.5787E + 01	453.0	0.6719E + 01	1902.963	68577.8
34.00	0.6402E + 01	461.1	0.7302E + 01	1903.651	68619.1
33.00	0.7070E + 01	468.8	0.7934E + 01	1904.317	68659.0
32.00	0.7795E + 01	476.8	0.8602E + 01	1905.030	68701.8
31.00	0.8581E + 01	485.0	0.9310E + 01	1905.770	68746.2
30.00	0.9431E + 01	493.1	0.1007E + 02	1906.552	68793.1
29.00	0.1035E + 02	500.9	0.1088E + 02	1907.349	68840.9
28.00	0.1134E + 02	509.4	0.1172E + 02	1908.169	68890.1
27.00	0.1241E + 02	517.7	0.1262E + 02	1909.035	68942.1
26.00	0.1356E + 02	526.6	0.1356E + 02	1909.953	68997.2
25.00	0.1480E + 02	535.4	0.1455E + 02	1910.920	69055.2
24.00	0.1612E + 02	543.5	0.1562E + 02	1911.867	69112.0
23.00	0.1755E + 02	552.3	0.1673E + 02	1912.873	69172.4
22.00	0.1907E + 02	560.7	0.1790E + 02	1913.936	69236.1
21.00	0.2070E + 02	568.8	0.1915E + 02	1914.979	69298.8
20.00	0.2245E + 02	577.0	0.2047E + 02	1916.092	69365.5
19.00	0.2431E + 02	585.5	0.2184E + 02	1917.255	69435.3
18.00	0.2630E + 02	593.5	0.2331E + 02	1918.443	69506.6
17.00	0.2842E + 02	602.0	0.2483E + 02	1919.688	69581.3
16.00	0.3068E + 02	610.7	0.2641E + 02	1921.036	69662.1
15.00	0.3308E + 02	618.7	0.2809E + 02	1922.375	69742.5
14.00	0.3564E + 02	626.7	0.2986E + 02	1923.684	69821.0
13.00	0.3836E + 02	634.8	0.3171E + 02	1925.002	69900.1
12.00	0.4124E + 02	643.5	0.3361E + 02	1926.515	69990.9
11.00	0.4430E + 02	651.5	0.3564E + 02	1928.033	70082.0
10.00	0.4754E + 02	659.4	0.3774E + 02	1929.631	70177.8
9.00	0.5097E + 02	667.3	0.3995E + 02	1931.224	70273.5
8.00	0.5461E + 02	675.2	0.4226E + 02	1932.999	70379.9
7.00	0.5845E + 02	683.0	0.4468E + 02	1934.729	70483.7
6.00	0.6252E + 02	690.8	0.4720E + 02	1936.538	70592.3
5.00	0.6681E + 02	698.5	0.4983E + 02	1938.346	70700.7
4.00	0.7134E + 02	706.2	0.5256E + 02	1940.210	70812.6
3.00	0.7612E + 02	713.9	0.5540E + 02	1942.041	70922.5
2.00	0.8116E + 02	721.5	0.5835E + 02	1943.904	71034.2
1.00	0.8647E + 02	729.1	0.6142E + 02	1945.830	71149.8
0.98	0.8658E + 02	729.3	0.6148E + 02	1945.858	71151.5

Altitudes are relative to the sounder probe landing site at 6052.0 km. $R_0 = 6053.0$ km, $g_0 = 8.8685$ m/s², $\mu = 43.44$. GRT 1853.405 = 18 hours, 53.405 minutes.

in Figure 10. They span 9 orders of magnitude, from 10^{-7} to 64 kg/m³. The comparison of data obtained by the two extremely different techniques provides a test of accuracy of the entry mode data above 65 km. In Figure 10a, where densities

below 65 km (filled symbols) were obtained from p , T measurements, the data from the two experiment modes fit together beautifully. Below 115 km, the day and sounder densities are the same within a few percent, while below 100 km

TABLE 4. Measured Planet Radii in Vicinity of Small Probe Landing Sites

Probe	Landed Radius, km	Terrain Elevation, Radar Altimeter, km	Terrain Elevation, Pressure Data, km
North	6053.5 ± 0.5	+1.5 ± 0.7	+1.08 ± 0.1
Day	6052.0 ± 0.5	0	0
Night	6051.5 ± 0.5	-0.5 ± 0.7	-0.55 ± 0.1

the north probe densities are lower by 20–33%. Densities from all three probes converge at 110 km, above which the day and north probe profiles diverge strongly, differing by a factor of 2 at 120 km. The small waviness in $\rho(z)$ results in more pronounced waviness in $T(z)$ seen in Figure 6. The largest density wave is just above 110 km and may be seen in both the day probe and north probe data.

The densities below 65 km, Figure 10b, include a correction for real gas effects by use of the NBS tables for CO₂ [Hilsenrath *et al.*, 1960]. The compressibility factor ζ in the equation of state varies from 1.01 at the planet surface to a minimum of 0.993 at 25–30 km. This small correction affects derived altitudes by ~0.28 km at 60 km. Altitudes are reduced, since $\zeta < 1$ above 8 km.

Densities in the lower atmosphere are found to be more uniform from probe to probe than either temperatures or pressures. Thus, for example, T and p differ appreciably in the north probe sounding from those of other probes above ~45 km, but the north probe densities agree with those from the other probes within 2% at 61 km. Thus the temperature and pressure differences are proportional, as they would be in the case of a constant volume process, such as quasi nondivergent large scale transport.

The entry pressure data, Figure 11, extend to a minimum of 10⁻⁴ mbar. Since they are computed from the densities with the assumption of hydrostatic equilibrium, the grouping of data from the three probes is similar to that of the density data. The indication of lower pressures at 60° latitude has possible significance for zonal winds in cyclostrophic balance, which we will examine. The continuity of pressures above 65 km with those from the descent mode is excellent.

Entry mode results are presented in the data tables, Table 8, for the three probes. Altitude intervals are 1 km to ~80 km, and then 2 km, so as to be comparable with altitude resolution in the north probe data.

CONTRASTS IN THE LOWER ATMOSPHERIC STRUCTURE

Comparison of the temperatures as a function of pressure measured at the four widely separated probe sites, shown in Figure 8, indicates that at pressures above about 400 mbar,

TABLE 5. Selected Planet Radii at the Four Probe Landing Sites and Pressure at the Mean Surface

Probe	Landed Radius, km	p_0 , bars	Terrain Elevation Relative to Sounder Landing Site, km
North	6053.0 ± 0.25	86.6	0.98
Day	6051.92	92.7	-0.10
Night	6051.37	95.8	-0.65
Sounder	6052.02	92.2	0.00
Planet mean	6051.39	95.7 ± 1.4	-0.63 ± 0.25

TABLE 6. Initial Conditions at 200 km

	V_E , km/s	γ_E , deg	GRT
Souder	11.5377	-32.37	1848:44.9
North	11.5372	-68.74	1852:52.8
Day	11.5371	-25.44	1855:31.0
Night	11.5375	-41.50	1859:19.2

GRT = 1848:44.9 = 18 hours, 48 min, 44.9 s.

the thermal contrast is small over wide reaches of the planet from the deep night side to the morning terminator, and from the equator to 60° latitude. If we examine the differences in detail, as in Figure 12, we see that they are typically 5 K or less at pressures between 1 and 25 bars. Contrasts are referenced to the sounder probe, which measured temperatures within 2.5 K of the day and night probe soundings at 0.4 to 5 bars, and within 5 K up to 25 bars. It is evident that the day and night probe profiles are similar over this range to within ~1 K. At pressures below 0.4 bar, which is in the region of strong solar absorption in the clouds [Tomasko *et al.*, 1979], the near equatorial sounder profile becomes systematically warmer than the mid-latitude soundings. Somewhat surprisingly, however, in the deep atmosphere, the atmosphere is found to be cooler near the equator than at mid-latitudes.

The 60° latitude sounding of the north probe shows very small contrast (~1 K) to the equatorial sounding at pressures from 4 to 25 bars. Below 4 bars pressure, it becomes as might be expected, progressively cooler, due to less insolation, and reaches a contrast of -23 K at 200 mbar.

Above 25 bars, temperature differences in the data tend to increase. This is associated with differences in the lapse rates in the deep atmosphere, and will be further discussed in the section on stability.

Temperatures from the four soundings are compared as a function of altitude in Figure 13. One curve has been drawn through the sounder data, and the north probe data fall close to it between 20 and 41 km. A second curve through the day probe data fits the night probe data almost equally well above 17 km up to 56 km. Relationships of the four soundings are similar to those discussed above, except that temperature differences at a given altitude are somewhat greater than those at a given pressure, because altitudes are increased by persistently higher temperature (2), and this adds to the temperature difference. Thus, in the altitude range from 50 to 56 km (middle cloud region [Knollenberg and Hunten, 1979]), the temperature at a given altitude differs by ~10 K between the north and day probe soundings, as compared to 6 or 7 K at a given pressure.

Contrasts in temperature as a function of altitude are shown explicitly in Figure 14. To show the very interesting day-night relationship, the day probe sounding was taken as reference, Figure 14a. On the basis of Figure 13, the near equality of temperatures at these two sites between 18 and 35 km was expected, but we were surprised to find a well defined wave appearing in the temperature differences above 35 km. Since these two probes were separated in longitude by 99.7°, a global scale phenomenon is implied. As we shall see, the lower altitude boundary of this wave is near the bottom of a deep stable layer in the lower atmosphere. Taken together, these observations suggest gravity waves with global organization. It is also significant that large oscillations in meridional flow velocities were observed at the day and night probe sites above 35 km [Counselman *et al.*, this issue].

The mean
km. T
tation
lower
long c
the pla
The
day-so
most i
tudes a
of the
compa
of con
becom
increas
We
temper

Fig. 9
try pro
tests in
models
Reynol
tack, <1
The effi
value, a
free mo

TABLE 7. Selected Atmospheric Mean Molecular Weights

	1	2	3	4	5	6	7	8
z , km	<80	90	100	110	115	120	125	130
$\mu(z)$, amu	43.44	43.4	43.2	43.0	42.8	42.5	42.2	41.7
$\mu(z)$, amu, BNMS model			43.2	42.8	42.3	41.8	41.0	39.8

The measured contrast is <2 K from 18 to 35 km, and the mean curve through the wave is comparably small up to 64 km. This is consistent with the pre-Pioneer Venus expectation of small day-night differences in temperature in the lower atmosphere, due to the thermal time constant being long compared with the time for zonal winds to move around the planet [e.g., Stone, 1975].

The wave structure is also apparent in the day-north and day-sounder contrasts, Figure 14b and 14c. It seems to be almost in phase with the day-night contrast wave. Wave amplitudes are 2.5–5 K, increasing with altitude, and wavelength is of the order of 10–15 km. In the day-north and day-sounder comparisons, the wave is superimposed on a mean variation of contrast with altitude, which is for the sounder profile to become warmer, and the north profile to become cooler with increasing altitude, above about 25 km.

We will return to a discussion of the Venera 10 sounder temperature comparison.

Pressures from the four soundings were plotted against altitude in Figure 7. At altitudes below 24 km, the single curve shown passes through the sounder data, and through data of the other three probes as well. The second curve started at 24 km passes through the day probe data. The pressure differences are of the order of a few percent below 50 km. Since these differences exceed the root sum square uncertainty in pressures of two probes (1.4%) by only a factor of 2 or 3, and the corresponding altitude difference at constant pressure is ~ 0.25 km at 50 km or 0.5%, no more than a factor of 2 greater than the estimated accuracy, it is not certain that the differences are real. The difference between the mid-latitude probe pressures and sounder pressures is in the direction expected from the temperature differences discussed earlier (i.e., p is higher for the probes at 30° latitude). It is also remarkable how closely the two probes at 30° latitude follow the same curve. The divergence of measured pressures at mid-latitudes from those of the other two probes increases gradually with increasing altitude. We are inclined to believe that these differences seen above 20 km are real.

The pressure differences are shown explicitly in Figure 15, referenced again to the day probe pressures. A build-up in day-night pressure difference to $\sim 1\%$ at 60 km is measured, but we do not believe that this is necessarily real, since 1% is the order of the pressure measuring accuracy, and a relative altitude accuracy of ~ 10 m at 60 km is necessary to define this difference significantly. However, the day-north pressure difference, which builds up to 9% at 61 km, and the day-sounder difference of 5% at 57 km should be significant. The day-north difference is smaller than in our preliminary report, but it is in the direction needed for cyclostrophic balance of zonal winds [Seiff et al., 1979b]. We will discuss this more fully in a later section. The day-sounder difference is opposite to the direction for cyclostrophic balance and would tend to accelerate the atmosphere equatorward. This is the mean direction of meridional flow observed at the day probe site in the data of Counselman et al. [this issue] at altitudes from 20 to 60 km.

The other interesting characteristic in the Δp data is that waves are again evident, and they are phase displaced by 90° from the temperature waves. For wavelengths less than or comparable to the scale height, a phase displacement of approximately 90° can be shown to be required by the equation of hydrostatic equilibrium.

LAPSE RATES AND CONVECTIVE STABILITY

To illustrate the detailed variations observed in $T(z)$, about every third data point from the sounder probe, which has much better altitude resolution than the small probes, is plotted in Figure 16. Pronounced changes in lapse rate are clearly evident, several of which can be correlated with the clouds and cloud boundaries, located at altitudes marked along the z axis. Straight lines indicating data slopes have been extended to facilitate visualization of the changes which were measured. In the middle cloud, for example, the lapse

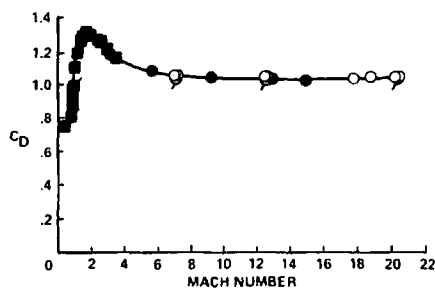


Fig. 9a

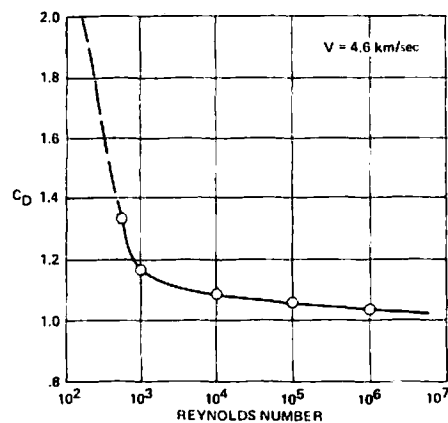


Fig. 9b

Fig. 9. Test data on the drag coefficient of the Pioneer Venus entry probes. (a) Variation with Mach number. Open points are from tests in CO_2 ; filled symbols, tests in air. Flagged symbols are from models of the sounder probe; unflagged symbols, small probe models. Reynolds numbers were between 5×10^3 and 3×10^6 . Angles of attack, $<11^\circ$. (b) Variation with Reynolds number at hypersonic speed. The effect of Reynolds number is moderate above 10^3 . Below that value, a rapid increase in C_D occurs. Data are extrapolated toward a free molecular flow value of 2.2.

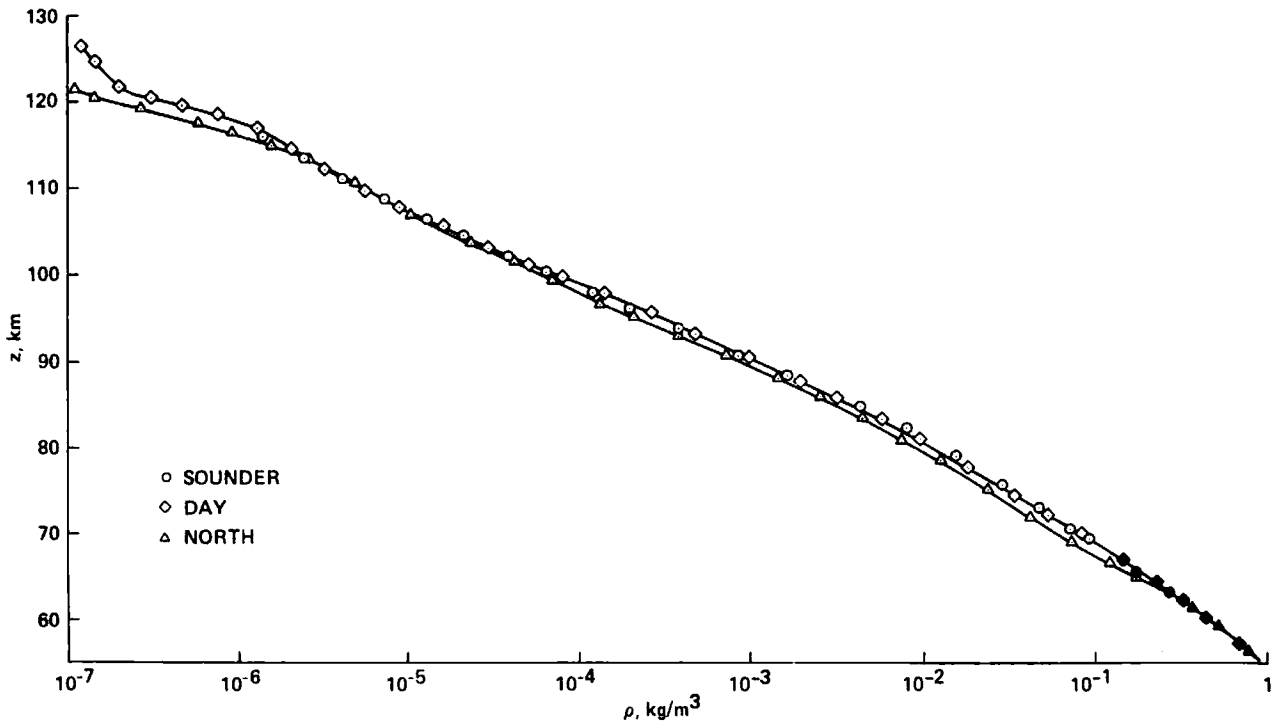


Fig. 10a

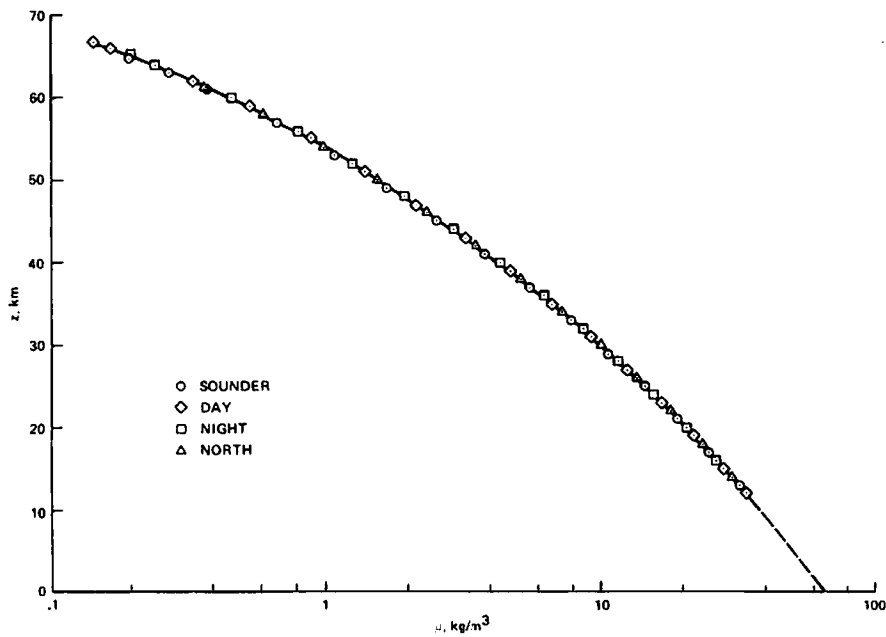


Fig. 10b

Fig. 10. Density profiles of the atmosphere from the surface to 126 km. Altitudes here and in all subsequent figures are relative to the sounder landing site, except where noted. (a) Entry data from probe deceleration measurements. Filled symbols are descent mode data included for comparison. (b) Descent mode data from measured pressures and temperatures and the equation of state. A single curve through day probe densities also fits the other three sets of data closely. Close agreement of north probe densities with those of the other probes at altitudes where temperatures differ implies effectively a constant volume process (i.e., $T \sim \rho$).

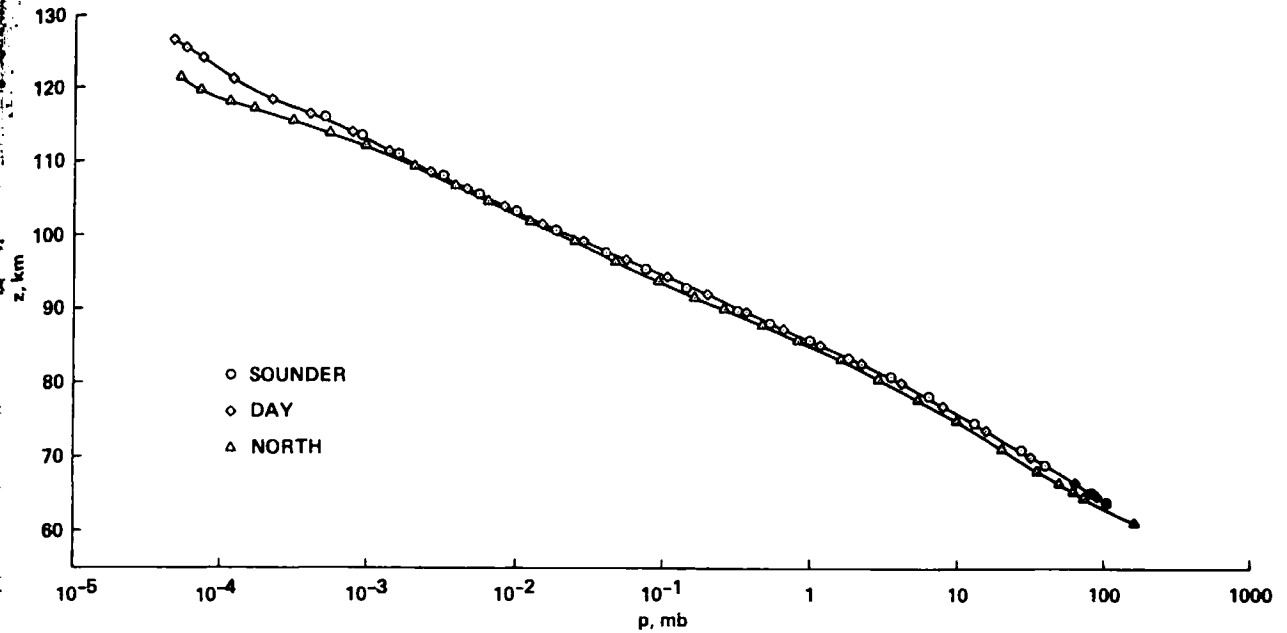


Fig. 11. Atmospheric pressures above 65 km from probe deceleration measurements. Filled symbols from pressure sensing in descent are included for comparison. The lower north probe pressures are in a direction to provide cyclostrophic balance of zonal winds up to an altitude of 105 km. Above 110 km, the temperature data (Figure 6) indicate the presence of wave phenomena, which are probably responsible for the pressure differences as well.

TABLE 8a. State Properties of the Middle Atmosphere of Venus: Pioneer Venus Sounder Probe

Altitude, km	p , bars	T , K	ρ , kg/m ³	GRT	GRT, s
116	0.5199E-06	190.2	0.1405E-05	1848.975	67738.5
114	0.8255E-06	190.2	0.2236E-05	1848.980	67738.8
112	0.1318E-05	190.2	0.3577E-05	1848.986	67739.1
110	0.2075E-05	194.4	0.5520E-05	1848.991	67739.5
108	0.3273E-05	196.3	0.8630E-05	1848.997	67739.8
106	0.5171E-05	190.1	0.1409E-04	1849.002	67740.1
104	0.8338E-05	183.0	0.2363E-04	1849.008	67740.5
102	0.1362E-04	180.7	0.3911E-04	1849.013	67740.8
100	0.2252E-04	174.1	0.6718E-04	1849.019	67741.1
98	0.3773E-04	173.3	0.1132E-03	1849.024	67741.5
96	0.6350E-04	168.9	0.1957E-03	1849.030	67741.8
94	0.1078E-03	168.9	0.3326E-03	1849.035	67742.1
92	0.1848E-03	167.1	0.5768E-03	1849.041	67742.4
90	0.3168E-03	165.4	0.9999E-03	1849.046	67742.8
88	0.5469E-03	165.2	0.1728E-02	1849.052	67743.1
86	0.9402E-03	163.8	0.2997E-02	1849.058	67743.5
84	0.1634E-02	164.7	0.5184E-02	1849.064	67743.8
82	0.2757E-02	181.1	0.7951E-02	1849.070	67744.2
80	0.4449E-02	195.8	0.1188E-01	1849.077	67744.6
79	0.5577E-02	204.1	0.1428E-01	1849.081	67744.8
78	0.6926E-02	212.4	0.1704E-01	1849.085	67745.1
77	0.8553E-02	215.1	0.2077E-01	1849.089	67745.3
76	0.1054E-01	216.9	0.2540E-01	1849.094	67745.6
75	0.1296E-01	221.1	0.3064E-01	1849.099	67746.0
74	0.1587E-01	227.3	0.3647E-01	1849.106	67746.4
73	0.1934E-01	227.8	0.4435E-01	1849.114	67746.8
72	0.2349E-01	233.5	0.5256E-01	1849.124	67747.4
71	0.2850E-01	234.9	0.6339E-01	1849.137	67748.2
70	0.3440E-01	243.5	0.7381E-01	1849.155	67749.3
69	0.4166E-01	230.5	0.9444E-01	1849.181	67750.8

$R_0 = 6052.0$ km, $g_0 = 8.2689$ m/s², $\mu = \mu(z)$ (Table 7). GRT 1848.975 = 18 hours, 48.975 min.

TABLE 8b. State Properties of the Middle Atmosphere of Venus: Pioneer Venus Day Probe

Altitude, km	p , bars	T , K	ρ kg/m ³	GRT	GRT, s
126	0.5046E-07	201.3	0.1269E-06	1855.767	68146.0
124	0.7428E-07	241.2	0.1565E-06	1855.774	68146.5
122	0.1038E-06	278.0	0.1902E-06	1855.781	68146.9
120	0.1470E-06	187.9	0.4001E-06	1855.788	68147.3
118	0.2542E-06	151.8	0.8584E-06	1855.795	68147.7
116	0.4571E-06	152.9	0.1537E-05	1855.802	68148.1
114	0.7732E-06	181.3	0.2197E-05	1855.809	68148.5
112	0.1229E-05	195.3	0.3249E-05	1855.816	68149.0
110	0.1913E-05	198.5	0.4984E-05	1855.823	68149.4
108	0.3013E-05	192.2	0.8117E-05	1855.830	68149.8
106	0.4823E-05	185.1	0.1350E-04	1855.837	68150.2
104	0.7813E-05	182.0	0.2226E-04	1855.844	68150.6
102	0.1275E-04	179.9	0.3680E-04	1855.851	68151.0
100	0.2140E-04	163.9	0.6785E-04	1855.858	68151.5
98	0.3757E-04	157.9	0.1237E-03	1855.865	68151.9
96	0.6621E-04	160.1	0.2153E-03	1855.872	68152.3
94	0.1143E-03	166.8	0.3571E-03	1855.879	68152.7
92	0.1946E-03	171.8	0.5905E-03	1855.886	68153.2
90	0.3271E-03	171.4	0.9964E-03	1855.893	68153.6
88	0.5469E-03	177.9	0.1605E-02	1855.900	68154.0
86	0.9156E-03	170.7	0.2801E-02	1855.908	68154.5
84	0.1539E-02	178.1	0.4515E-02	1855.916	68154.9
82	0.2522E-02	184.6	0.7135E-02	1855.924	68155.4
80	0.4040E-02	198.3	0.1065E-01	1855.933	68156.0
79	0.5052E-02	205.5	0.1284E-01	1855.938	68156.3
78	0.6279E-02	209.4	0.1567E-01	1855.943	68156.6
77	0.7788E-02	209.4	0.1943E-01	1855.949	68156.9
76	0.9655E-02	211.5	0.2385E-01	1855.956	68157.4
75	0.1193E-01	216.5	0.2878E-01	1855.964	68157.8
74	0.1466E-01	222.3	0.3445E-01	1855.973	68158.4
73	0.1795E-01	223.0	0.4204E-01	1855.985	68159.1
72	0.2196E-01	225.3	0.5093E-01	1856.001	68160.1
71	0.2674E-01	231.9	0.6025E-01	1856.023	68161.4
70	0.3257E-01	219.3	0.7758E-01	1856.055	68163.3

The altitude reference is the sounder probe landing site at 6052.0 km. $R_0 = 6051.9$ km, $g_0 = 8.8697$ m/s², $\mu = \mu(z)$ (Table 7). GRT 1855.767 = 18 hours, 55.767 min.

rate is close to adiabatic but increases gradually with altitude ($T(z)$ is gently curving). At the middle cloud upper boundary, 56 km, dT/dz makes a sudden stable change as the upper cloud is entered. Slope changes occur at both boundaries of the lower cloud. At $T = 273$ K, $z = 58$ to 59 km, dT/dz levels off for an altitude interval of about 1 km. This slope change, which is also seen in Figure 1, suggests a phase change process, perhaps H_2SO_4 freezing (freezing point of 80% H_2SO_4 is

270 K). The obvious candidate for phase change at 273 K, water, may not be supportable if the atmosphere is as dry as reported by other investigators [Moroz *et al.*, 1979]. A second, small ledge in the $T(z)$ data is seen at 256 K at 61 km. Above 59 km, the lapse rate is higher than below 58 km, but still stable. It gradually decreases up to 64 km.

Below the middle cloud, between 49 and 50 km, there is a brief interval of increased stability at the boundary between middle and lower clouds. In the lower cloud, stability is again reduced. Below the clouds the atmosphere becomes highly stable, in a pronounced and easily visible change in lapse rate. This stable region persists down to ~ 28 km.

In the region from 44 to 48 km, the temperature data show visibly greater randomness than elsewhere, with random deviations up to 1 K. This is suggestive of turbulence. The scale is ~ 100 m or less. The altitude region is that of the lower turbulent layer (now more probably identified as a trapped gravity wave layer) seen by Woo *et al.* [1979, this issue]. A second, similar region of increased temperature randomness, also ~ 1 K, is seen in the sounder data at temperatures from 500 to 590 K (29 to 18 km). This lies in the region of neutral static stability to be described below, and probably indicates convective overturning. This layer lies below the altitude of critical refraction and is inaccessible to the radio occultation experiments.

This detailed examination of $T(z)$ establishes the basis for stability profiles discussed below. The variations described are clearly present in the data, and are not small or subtle effects.

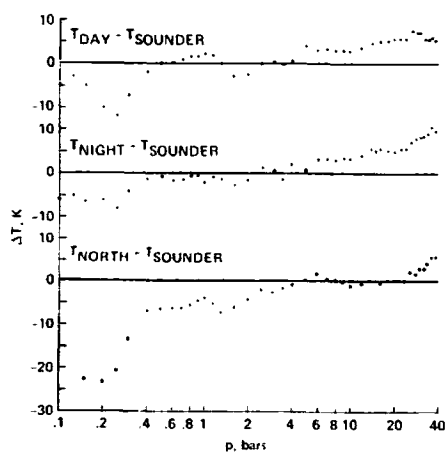


Fig. 12. Temperature contrasts as a function of pressure. The sounder temperature profile is used as reference.

TABLE 8c. State Properties of the Middle Atmosphere of Venus: Pioneer Venus North Probe

Altitude, km	p , bars	T , K	ρ , kg/m ³	GRT	GRT, s
120	0.6933E - 07	209.0	0.1696E - 06	1853.001	67980.1
118	0.1235E - 06	126.2	0.5015E - 06	1853.004	67980.3
116	0.2582E - 06	118.9	0.1116E - 05	1853.007	67980.4
114	0.5291E - 06	126.6	0.2154E - 05	1853.010	67980.6
112	0.1040E - 05	138.2	0.3885E - 05	1853.013	67980.8
110	0.1851E - 05	173.1	0.5530E - 05	1853.017	67981.0
108	0.3015E - 05	190.2	0.8205E - 05	1853.020	67981.2
106	0.4788E - 05	187.7	0.1322E - 04	1853.023	67981.4
104	0.7643E - 05	187.2	0.2118E - 04	1853.026	67981.5
102	0.1247E - 04	178.8	0.3620E - 04	1853.029	67981.7
100	0.2067E - 04	178.6	0.6013E - 04	1853.032	67981.9
98	0.3383E - 04	178.4	0.9865E - 04	1853.035	67982.1
96	0.5492E - 04	185.0	0.1545E - 03	1853.038	67982.3
94	0.9039E - 04	178.6	0.2638E - 03	1853.041	67982.5
92	0.1529E - 03	163.4	0.4882E - 03	1853.044	67982.7
90	0.2678E - 03	158.4	0.8825E - 03	1853.047	67982.8
88	0.4649E - 03	166.9	0.1454E - 02	1853.051	67983.0
86	0.7932E - 03	169.5	0.2443E - 02	1853.054	67983.2
84	0.1330E - 02	181.3	0.3831E - 02	1853.057	67983.4
82	0.2141E - 02	196.4	0.5695E - 02	1853.060	67983.6
80	0.3369E - 02	202.3	0.8700E - 02	1853.064	67983.8
79	0.4201E - 02	206.2	0.1064E - 01	1853.065	67983.9
78	0.5221E - 02	209.7	0.1300E - 01	1853.067	67984.0
77	0.6458E - 02	215.0	0.1570E - 01	1853.069	67984.1
76	0.7953E - 02	219.2	0.1896E - 01	1853.071	67984.3
75	0.9752E - 02	224.1	0.2273E - 01	1853.073	67984.4
74	0.1190E - 01	229.7	0.2706E - 01	1853.075	67984.5
73	0.1447E - 01	232.9	0.3245E - 01	1853.078	67984.7
72	0.1756E - 01	233.5	0.3929E - 01	1853.080	67984.8
71	0.2132E - 01	232.8	0.4785E - 01	1853.083	67985.0
70	0.2592E - 01	231.3	0.5853E - 01	1853.086	67985.2
69	0.3152E - 01	232.3	0.7088E - 01	1853.090	67985.4
68	0.3821E - 01	235.3	0.8482E - 01	1853.095	67985.7
67	0.4650E - 01	225.8	0.1076E + 00	1853.101	67986.1
66	0.5733E - 01	205.6	0.1457E + 00	1853.110	67986.6
65	0.7108E - 01	222.9	0.1666E + 00	1853.123	67987.4

The altitude reference is the sounder probe landing site at 6052.0 km. $R_0 = 6053.0$ km, $g_0 = 8.8665$ m/s², $\mu = \mu(z)$ (Table 7). GRT 1853.001 = 18 hours, 53.001 min.

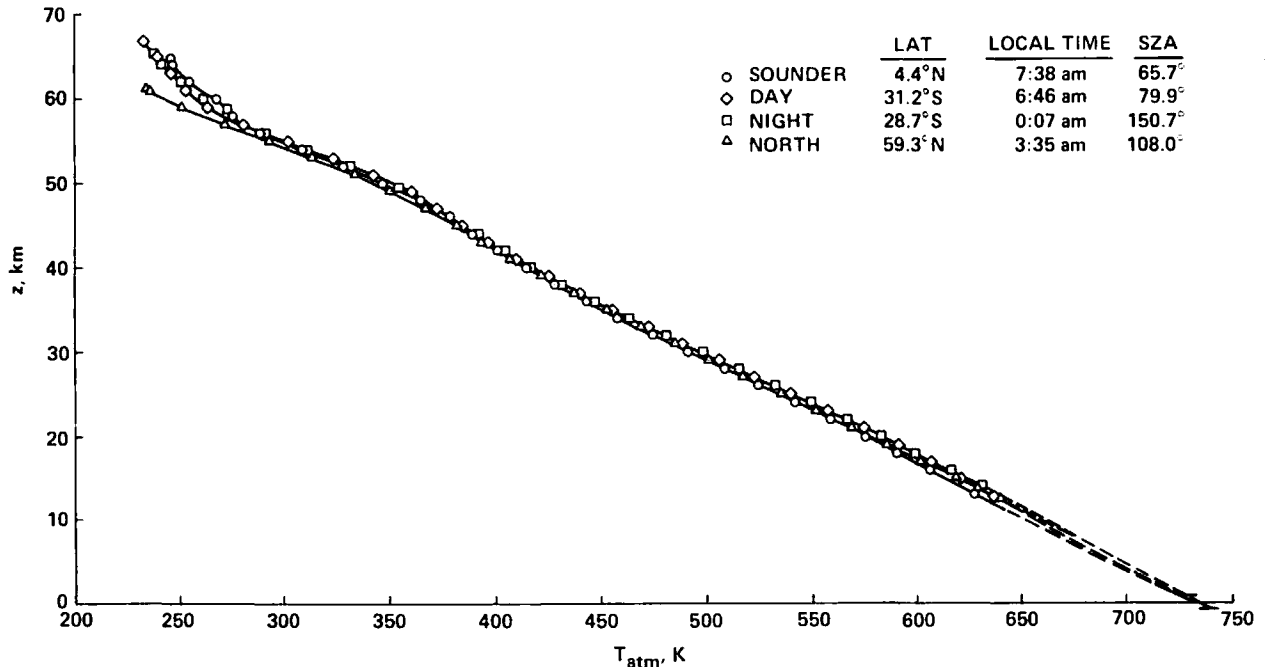


Fig. 13. Comparison of temperature profiles from the four probes below an altitude of 65 km. This may be compared with the preliminary data in Figure 1 of Seiff et al. [1979b], which showed close agreement of the four profiles, but the more complete analysis has brought them even closer together. SZA is solar zenith angle.

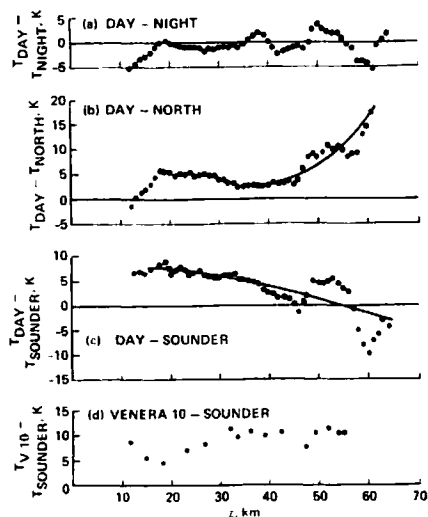


Fig. 14. Thermal contrasts as a function of altitude, among the four Pioneer Venus probe soundings of the lower atmosphere, and temperature differences between the sounder probe and Venera 10. The waves which appear in the Pioneer Venus data above about 35 km altitude suggest the presence of gravity waves of global extent (see text).

The small probes show similar variations, but with less altitude resolution. The north probe data essentially overlies the sounder data below 43 km, but differ substantially from those of the sounder in the middle and upper cloud regions, as noted earlier. The lapse rate profiles, however, are similar through the middle cloud, as shown in Figure 17 which presents the vertical profiles of static stability from the four probes. The lapse rates shown by the curves were computed from the pressure and temperature data and the equation of hydrostatic equilibrium. The procedure used was to fit a cubic spline curve to $T(p)$ data points over altitude intervals of either 2 or 4 km, and to calculate dT/dz from $-\rho g(dT/dp)$ where dT/dp was local slope of the fitted curve. The intersections of the fitted curves in adjoining intervals were required to be continuous in slope and curvature. Results of the 2 and 4 km interval fits were generally similar, but they differed in their resolution of regions of rapid change in dT/dz . They were used jointly to define the curves shown in Figure

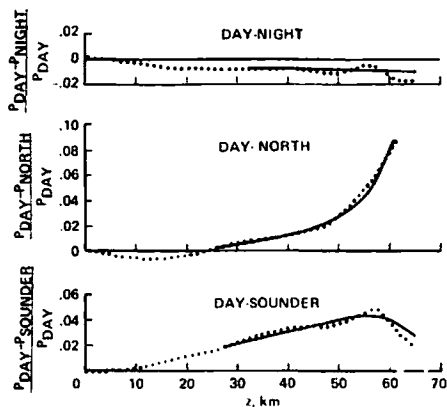


Fig. 15. Pressure differences among the four soundings in the lower atmosphere. Each of the difference curves exhibits a slow variation with an oscillation superimposed. The oscillation is 90° out of phase with the temperature waves of Figure 14.

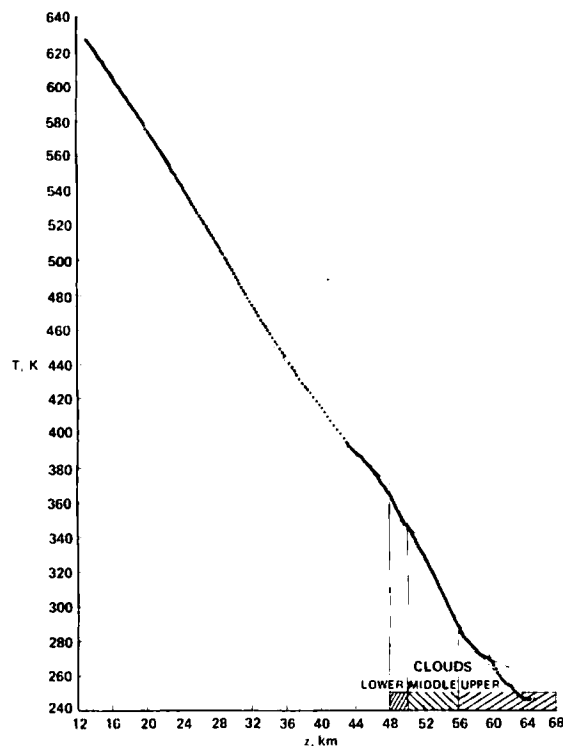


Fig. 16. Higher resolution plot of the sounder temperature data. Variability of the lapse rate is immediately apparent. Some changes occur abruptly at the independently identified cloud boundaries. There is a strongly stable change in lapse rate beginning just below the clouds. A second, smaller, stable change in lapse rate may be seen just below 20 km.

17. The data are cut off below 14 km since, in general, slopes cannot be well determined near the end of a set of data. The upper altitude limit to the curves was set mostly by the fact that dynamic corrections to temperature and pressure arising from the small probe trajectory velocities became large near 60 km. The points in Figure 17 are from lapse rates read graphically by taking local slopes on $T(z)$ plots, such as those slopes indicated in Figure 16, and generally confirm the results of the spline fitting procedure. The graphical method permits human judgment to be applied in observing where sudden slope changes occur, etc., but is subject to uncertainty in placing a tangent to the curve locally (over 2 km intervals or less).

The adiabatic lapse rates used in deriving Figure 17 were computed for pure CO_2 and for a mixture of 0.965 CO_2 and 0.035 N_2 from the relation

$$\Gamma = -(\alpha T) \frac{g}{c_p} \quad (7)$$

in which $c_p = c_p(T, p)$ [Hilsenrath et al., 1960], $g = g(z)$, and αT , which is unity for a perfect gas, was evaluated from

$$\alpha = -\frac{1}{\rho} \left(\frac{\partial \rho}{\partial T} \right)_p \quad (8)$$

(See Staley [1970] for a complete discussion of Γ including nonideal gas effects for CO_2 at Venus pressures and temperatures.) The partial derivative in (8) was also evaluated from the Hilsenrath [1960] tables. The αT correction factor ranges

Fig
probe
cubic
from

from
ure l
range
woul
conca
Th
of on
c_p an

wher
tion
woul
at th
quire
in its
ever,
the r
Th
tanti
order
two
gene
The

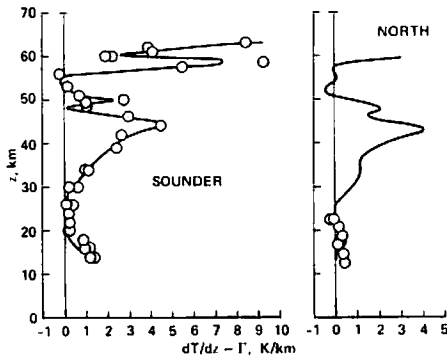


Fig. 17a

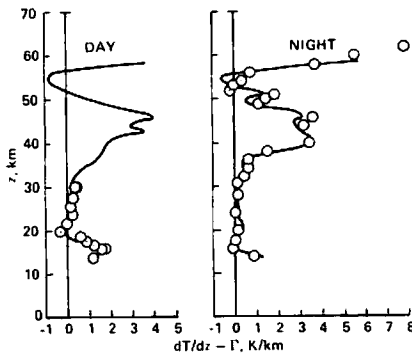


Fig. 17b

Fig. 17. Profiles of static stability of the atmosphere at the four probe entry sites. Positive values indicate stability. Curves are from cubic spline fits to the data. Points indicate slopes taken graphically from $T(z)$ plots.

from 1.01 to 1.09. Results of the calculations are shown in Figure 18. The adiabatic lapse rate varies by about 30% over the range of temperatures found in the lower atmosphere, which would, of course, cause $T(z)$ in an adiabatic atmosphere to be concave downward (compare with Figure 6).

The presence of 3.5% N_2 is estimated to cause a change in Γ of only a few hundredths K/km, typically. The effect of N_2 on c_p and T was estimated by assuming

$$c_p = \sum_i n_i c_{p,i} \quad (9)$$

$$\alpha T = \sum_i n_i (\alpha T)_i \quad (10)$$

where n_i is the mole fraction of species i (N_2 or CO_2). (Equation (10) is not rigorous, since N_2 in a bath of mostly CO_2 would exhibit different gaseous imperfections than in pure N_2 at the same total pressure. To treat this problem exactly requires that imperfect gas properties of the mixture be derived, in itself a research task. Since the N_2 fraction is small, however, and the αT correction magnitude is moderate, we believe the remaining uncertainty is small.)

The uncertainty in the stability due to measurement uncertainties, etc., is hard to define quantitatively, but is of the order of a few tenths K/km. The agreement between the two independent procedures for defining the lapse rates is generally within a few tenths K/km, often, within 0.1 K/km. The local slope technique applied to the sounder data defines

a more nearly discontinuous change at the boundary of the middle and lower clouds (which appears from the data to be real) and at the 60 km level where the 273 ledge occurs. (This is a resolution difference between the techniques.)

Both techniques show a tendency for the lapse rate to become stable again below 20 km, with stability ~ 1 K/km on three of the four probes. (The north probe data do not show this to the same degree.) This tendency is real in the data. We were concerned with the possibility that it is a precursor effect of the sensor breakdown which occurred at 12.5 km. Nothing in the data particularly supports this concern, however. In the sounder $T(z)$ data, Figure 16, a slope change just below 20 km at 580 K can be clearly identified. During this period in the deep atmosphere on all four probes, the temperature calibration reference reading remained normal, giving no suggestion of incipient breakdown. After breakdown, the reference readings dropped by hundreds of counts.

The stability profiles still support our earlier conclusions that there is a deep stable layer in the atmosphere of Venus extending from ~ 28 or 30 km into the middle cloud and that the clouds control the stability between approximately 45 km altitude and the cloud tops [Seiff *et al.*, 1979b]. The slightly unstable or neutrally stable region between 50 and 55 km is planet wide and occurs in the middle cloud region. The inflections in the sounder, night, and north probe profiles between 45 and 55 km seem to be correlated, as stated earlier, to the boundary of the lower cloud and middle cloud regions as determined from the 175° back scattering cross section measured by the probe nephelometers [Blamont and Ragert, 1979]. The significant difference in stability of the day probe from the other probes between 46 and 50 km appears to be correlated with slight differences in cloud structure seen by the nephelometers; that is, the middle cloud lower boundary is at a higher altitude for the day probe and the lower cloud appears less pronounced [Blamont and Ragert, 1979].

The interesting feature of the stability curves which we have not discussed in previous presentations of the data is the stable region below 20 km. Note that the day probe profile, and to a lesser extent the north probe profile, indicate that this stable region may be localized in altitude.

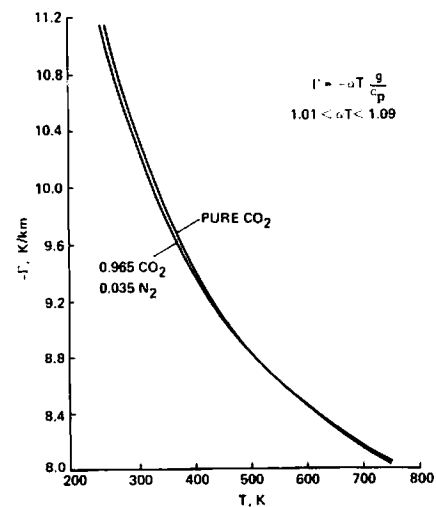


Fig. 18. Adiabatic lapse rates calculated for pure CO_2 and a 0.965 CO_2 , 0.035 N_2 mixture. The independent variable, temperature, also implies a pressure variation according to $T(p)$ measured by the sounder in the Venus atmosphere. Real gas effects are included (see text).

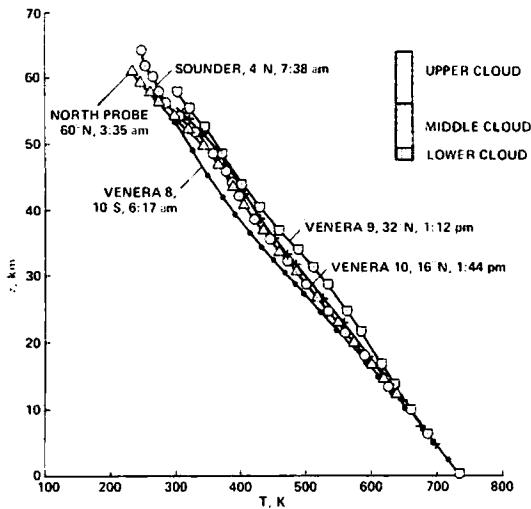


Fig. 19. Comparison of Venera 8, 9, and 10 temperature profiles with those of Pioneer Venus probes. Altitude reference, $z = 0$, is taken at the 91.0 bar level.

Under reasonable assumptions as to atmospheric and cloud composition, radiative thermal balance models [Tomasko *et al.*, 1979; Pollack *et al.*, this issue] give qualitatively similar stability profiles above 35 km as those presented in Figure 17. More difficult to understand is the stable region below 20 km. If infrared radiative processes are the cause, infrared opacity must decrease toward the surface, at least for a certain altitude range below ~ 20 km. It may be that the shift in the black body spectrum at higher temperatures plays some role in creating the stable region [Pollack *et al.*, this issue]. If large-scale dynamics is the cause, the motion fields must be capable of producing static stabilities with $(dT/dz - \Gamma) \sim 1$ K/km, which seems large in light of previous analyses [e.g., Stone, 1974].

COMPARISONS WITH VENERA PROBE MEASUREMENTS AND OTHER PIONEER VENUS EXPERIMENTS

A comparison of the thermal structure below 54 km altitude as determined by Venera 8 [Marov *et al.*, 1973], Venera 9, and Venera 10 [Avduvskii *et al.*, 1976], and the Pioneer Venus north probe and sounder probe is presented in Figure 19. The Venera 8 comparison is interesting because it was the Venera probe nearest the latitude and entry time of the sounder probe [cf. Colin, this issue]. The Venera 9 and 10 comparisons are of interest because they were soundings in the midday region of the planet, inaccessible to Pioneer Venus. The general nature of the temperature profiles is similar, the correspondence between the sounder probe and Venera 10 being very close, but important differences exist in thermal contrast magnitudes and in stability. The Venera 8 lapse rates differ appreciably from those of Pioneer Venus, being less stable at low altitudes, and more stable at high altitudes. Conversely, Venera 9 lapse rates are more stable than Pioneer Venus at low altitudes. Temperature differences between the Venera and Pioneer Venus profiles reach ~ 25 K, at 45 km altitude for Venera 8 and at 30 km for Venera 9. The temperature differences between Veneras 8 and 9 is ~ 50 K from $z = 25$ to 50 km.

On the other hand, the similarities between the Venera 10 and sounder temperature profiles are striking, in that both exhibit the same curve shapes and inflections. Temperature dif-

ferences between these two soundings were included in Figure 14d, where it is seen that the Venera 10 profile was 5–10 K warmer than the sounder profile. This should not be interpreted as contrast, however, because the soundings were not simultaneous, nor were they made with similar instruments, carefully intercalibrated, and similarly deployed, etc. Nevertheless, at its face value, the comparison indicates a warmer atmosphere in early afternoon than in early morning.

The Venera 9 sounding, at approximately the same local time as Venera 10, but at 32° latitude compared to 16° , is 22 K warmer than Venera 10 at 30 km. This compares to the mid-latitude soundings being 5 K warmer than the equatorial sounding of Pioneer Venus, but it is interesting that the sense of the relationship is the same.

How significant the differences are between the Venera probes and Pioneer Venus probes is open to question. The stated uncertainties in temperature measurements of the Venera probes is about $\pm 1.5\%$ or ± 2 K to ± 9 K [Kuzmin and Marov, 1974; Marov *et al.*, 1973]. There are also significant altitude uncertainties discussed by Marov *et al.* [1973] for Venera 8, ± 3 km, which in light of a lapse rate of ~ 8 K/km, could introduce temperature discrepancies of ± 25 K. These uncertainties, coupled with those stated earlier for the Pioneer Venus temperatures and altitudes, would appear capable of explaining discrepancies in static stability and differences in detailed shape of the temperature profiles. The large temperature differences between Venera 9 and 10 may also be due in part to measurement uncertainties. An alternative explanation is that considerable temporal variations in the thermal structure occur. However, Venera 9 and 10 entered the atmosphere of Venus separated in time by only about 3 days, and a 20 K difference occurring at 30 km in about 3 days as indicated by Venera 9 and 10 is hard to reconcile with the thermal time constants at these levels. For example, the radiative time constant at 30 km is the order of 3000 days [Pollack and Young, 1975]. Hence we believe measurement uncertainties to be the necessary explanation, and this makes it impossible to assign quantitative significance to the Venera 10-sounder differences.

Comparisons of data from the orbiter radio occultations with the present data are shown in Figure 20, for the latitude of the north probe, $60^\circ \pm 6^\circ$ (orbits 18 X and 60 N, A. Kliore,

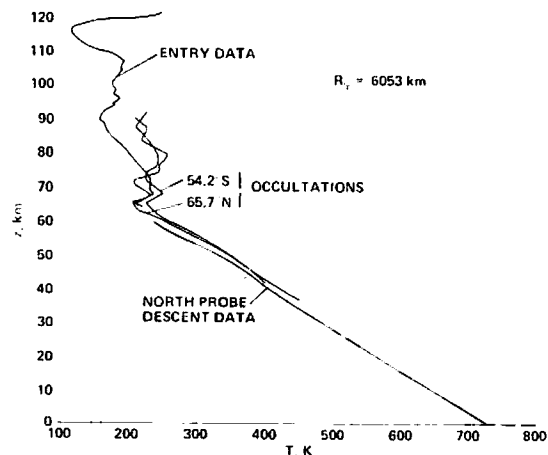


Fig. 20. Comparison of radio occultation temperature profiles with those from the north probe sounding at 60° latitude. $z = 0$ at $R_0 = 6053.0$ km, the adopted north probe landing site elevation.

Fig. the sur Pioneer and the times r

private the de occult stability measurements unexp Venus is also two o agree cultati altitud

Cor those orbite This t from We ha data to with o of two taken cal Ve Elson, taken tudes, found of the below entry s itudes.

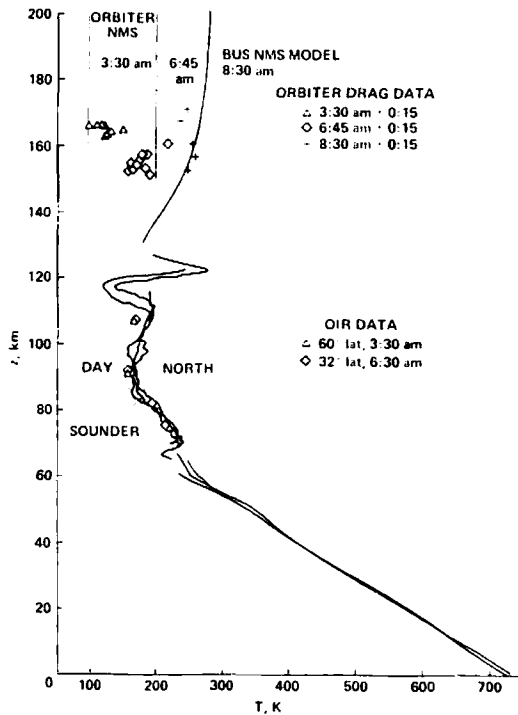


Fig. 21. Temperature structure in the atmosphere of Venus from the surface to an altitude of 200 km, as defined by five independent Pioneer Venus experiments, of which four are in situ measurements and the fifth, the OIR experiment, is remote sensing. Local Venus times represented are from 3:30 A.M. to 8:30 A.M.

private communication, 1979). The shape and curvature of the descent profile at 40–60 km are almost duplicated by the occultation data, which therefore can be said to confirm the stability results reported herein. Below 70 km, the two experiments seem to have an altitude displacement of 2 or 3 km of unexplained cause, even though both are referred to the same Venus radius, 6053 km. The inversion which we see at 65 km is also clearly seen in the occultation data. Above 75 km, these two occultations, one of which is one-way Doppler, did not agree as closely with our measurements. There are other occultations in which the agreement does extend to these higher altitudes [Kliore and Patel, this issue].

Comparisons of the entry probe temperature structure with those obtained by the orbiter infrared radiometer (OIR) and orbiter and bus in situ measurements are made in Figure 21. This figure summarizes vertical temperature structure data from Pioneer Venus. The OIR data are basically $T(p)$ data. We have used our $p(z)$ data, Figure 11, to convert the OIR data to $T(z)$, and thus put them on a common altitude basis with our measurements. This has been done for the averages of two OIR 60° latitude and of two 32° latitude measurements taken 1 day before and 1 day after the entries occurred, at local Venus times within ± 12 min of the probe entry time (Lee Elson, private communication, 1979). These OIR soundings taken 2 earth days apart differed by < 1 K at the lower altitudes, and by 8 K at the highest altitude where OIR typically found variability from sounding to sounding. The agreement of these data with our entry mode data is within about 10 K below 100 km, and within 20 K at 107 km. The north probe entry sounding is warmer than soundings at the two lower latitudes. This supports the warming trend with increasing lati-

tude seen in the OIR data generally. All of these data define the stratospheric temperatures to be within a narrow band (typically 10 or 15 K), below 110 km. The largest spread is 30 K, occurs at 97 km, and is attributable to temperature waves indicated in the day and north probe profiles.

In the upper atmosphere the temperatures show large diurnal changes [Keating et al., 1979a, b, 1980; Niemann et al., 1979, this issue]. There must therefore be a region of temperature adjustment between 140 and 120 km to allow the relatively invariant atmosphere temperatures at lower levels to join with the diurnally varying temperatures of the upper atmosphere. The region is not well defined by the data, the closest approach being between the in situ entry data of the day probe, which reached up to 125 km and the bus neutral mass spectrometer data, which reached down to 130 km [von Zahn et al., 1979, this issue]. Both of these experiments showed the presence of a sizeable temperature wave (at least ± 50 K amplitude) in the region where they were coming together, more specifically from 112 to 140 km. This wave may be induced by flow through the sudden density and temperature jumps which occur at the morning and evening terminators (observed by Keating et al. [1980]; and Niemann et al., [this issue]). Only the mean curve through the temperature wave is shown in the BNMS data in Figure 21, and it is directed at its lower altitudes toward the center of the temperature waves in the probe entry data.

Temperature data from the orbiter atmospheric drag experiment (OAD) are shown for the night side at the clock hours of the north and day probes and the bus entry. These data also have given evidence of temperature oscillations of ± 30 K amplitude [Keating et al., 1979b] which accounts for the data spread at a given clock hour. Finally, the orbiter neutral mass spectrometer (ONMS) temperatures are shown for two local times corresponding to day and north probe entries [Niemann et al., this issue]. These data fall near the cooler and warmer extremes, respectively, of the OAD temperatures, while confirming the sharp variation from day to night, and the temperature magnitudes.

The density profiles from 60 to 190 km altitude defined by data from these same experiments are compared in Figure 22. The strong diurnal variation in the upper atmospheric density [Keating et al., 1979a, b, 1980] appears to diminish and converge near an altitude of 115 km, below which $\rho(z)$ from three of the probes show much smaller variations. The transient, wave-induced density oscillations, and the dynamical pressure differences (see below) seem to be the main sources of variation from sounding to sounding below 120 km.

WIND MEASUREMENTS AND DYNAMICAL INFERENCES FROM THE STRUCTURE DATA

Winds in the lower atmosphere below 65 km were determined from Doppler tracking data analyzed by means of numerical reconstruction of the descent trajectory. This is an independent and separate method of wind determination from that of the DLBI experiment [Counselman et al., 1979, this issue] in the sense that the method of analysis is quite distinct and the winds are computed from only the Doppler component of the radio tracking data. The Doppler technique alone cannot separate zonal and meridional wind contributions. However, because of fortuitously favorable viewing geometry (see Table 9) the zonal wind was dominant in the data for three of the probes, and meridional wind was dominant in the viewing direction for the fourth.

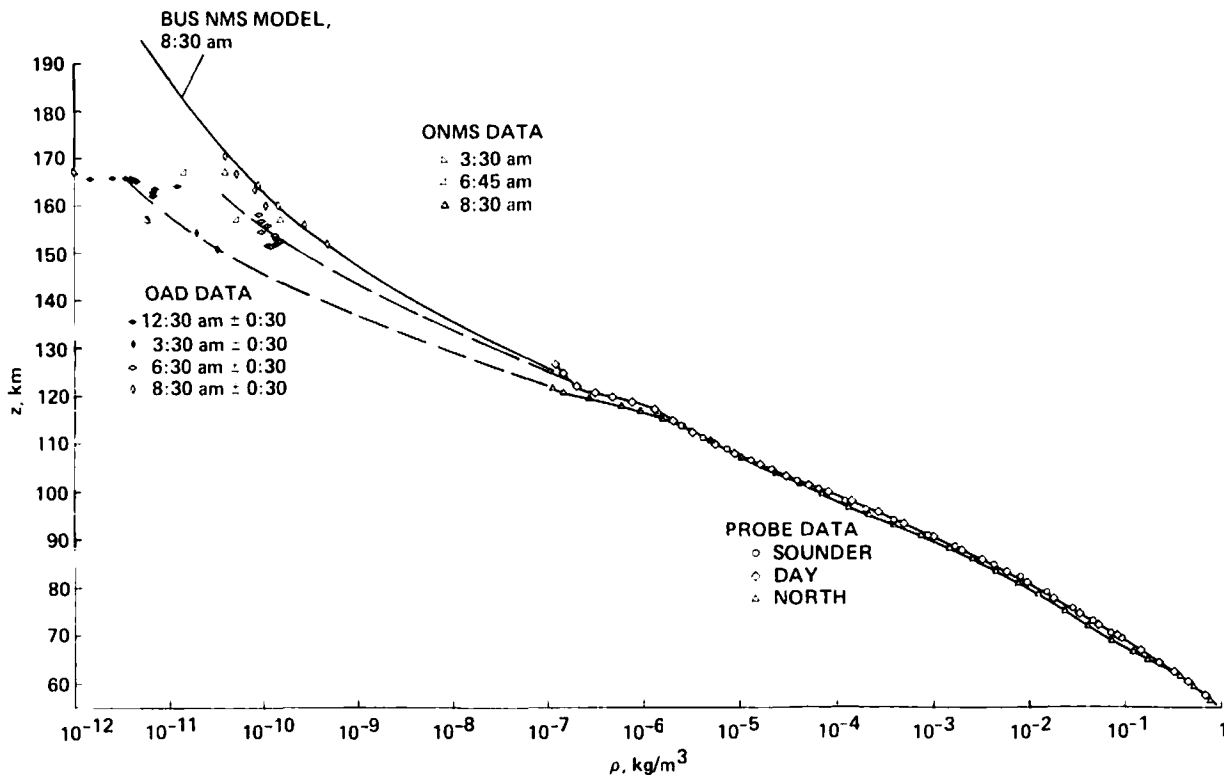


Fig. 22. Density structure of the atmosphere of Venus from 55 to 190 km from four independent experiments. Clock hours represented are from 12:30 A.M. to 8:30 A.M.

The approach is first to predict the descent trajectory in three dimensions from the initial conditions and a model of the atmosphere for the case of no winds. The 'model' of the lower atmosphere below 65 km was provided by measurements of T and ρ as functions of altitude, described earlier. Doppler shifts for this trajectory are then computed, and compared with those observed. If the differences (residuals) are larger than the expected Doppler noise (0.2 Hz), the difference is attributed to winds, and a wind profile is sought to minimize the sum of the squares of the Doppler residuals. The functional form which has been assumed for the wind profiles is linear between a finite number of fixed altitude points, usually spaced at 5 km intervals. An example of this process, for the day probe, is shown in Figure 23. Doppler residuals without winds ranged up to 570 Hz. With the winds modeled, residuals were reduced to ± 25 Hz. It is probable that a more detailed wind model would further reduce the residuals, which are oscillatory, in part, because of the piecewise linear nature of the wind model imposed. In the analysis, the vertical component of velocity is a known input, defined by prior analysis of the pressure and temperature data. After allowance for the descent velocity, it is assumed that the measured horizontal wind is entirely due to the direction of greatest measuring sensitivity (i.e., the zonal direction for the day, night, and sounder probes, and the meridional direction for the north probe). The trajectory analysis aspect was very important at the higher altitudes, where residual probe horizontal velocity must be carefully distinguished from wind velocity. Note that in this analysis, no assumption is made or needed relative to the advection of the probe by the winds. The probe's dynamical response to the winds is modeled by the trajectory equations.

Zonal winds derived from the day, night, and sounder probe data are shown in Figure 24, and compared with DLBI measurements of zonal winds [Counselman *et al.*, this issue]. The data extend up to about 63 km for the day probe and about 61 km for the night probe. Beyond these altitudes, no Doppler measurements are available. (Doppler data points for the day and night probes are not shown below 40 km, but they continue to agree closely with DLBI at these altitudes.) The close comparisons between the Doppler and DLBI solutions for zonal winds provide substantial evidence of the existence and character of the wind profile.

Of the three probes represented in Figure 24, the day probe measurement has the greatest sensitivity to meridional winds. If there were a 20 m/s meridional velocity present at the day probe site, it would contribute an incremental Doppler velocity of 7.2 m/s, which would be interpreted as a zonal velocity increment of $7.2/0.66$ or 10.8 m/s. Hence, the derived zonal velocity is relatively insensitive to the presence of meridional

TABLE 9. Sensitivities of the Measured Doppler Velocities to Meridional, Zonal, and Vertical Velocity Components

	$\frac{\partial U_D}{\partial V}$	$\frac{\partial U_D}{\partial U}$	$\frac{\partial U_D}{\partial V_d}$
Sounder	0.06	0.83	0.55
Day	0.36	0.66	0.66
Night	0.25	0.81	0.53
North	0.87	0.05	0.50

U_D is the Doppler component of the resultant velocity, while U , V , and V_d are the zonal, meridional, and descent components of probe velocity. A value of $\partial U_D/\partial V = 0.06$ means, e.g., that for $\Delta V = 10$ m/s, $\Delta U_D = 0.6$ m/s.

Fig. probe, far exc altitud

winds pler z that m less. (The m to we winds Since sugges pende

The the ear dional which probe in Fig son. T the str

The mode magn are on limit gested probe stable sult o km, t cillate m/s.

Me Doppr the d ties. I may studi

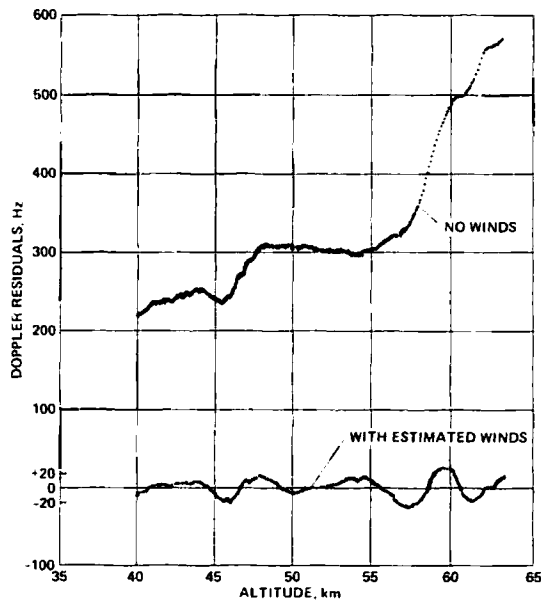


Fig. 23. Doppler residuals of the modeled trajectory of the day probe, with and without winds modeled. The residuals without winds far exceed those expected. The wind model, which is linear over 5 km altitude intervals, reduces residuals to ± 25 Hz.

winds even for this probe. The close comparison of the Doppler zonal velocities with the DLBI zonal velocities indicates that meridional velocities are small, of the order of 10 m/s or less. (This is also shown, of course, directly by the DLBI data.) The major wind field is therefore westward, that is, from east to west. Comparison of day probe winds with night probe winds indicates relatively little change in profile character. Since both probes are near the same southern latitude, this suggests that the zonal wind field is essentially diurnally independent, at least in these two samples.

The sounder probe Doppler data have the best visibility for the east/west velocity component and least sensitivity to meridional flow. In addition, they are two-way coherent data which are inherently much more accurate than the small probes' one-way radio data. Results presented for this probe in Figure 24 are for the period of free fall after parachute jettison. The data again agree closely with DLBI winds and show the strong wind shear which is present between 10 and 25 km.

The Doppler residuals of the north probe with no wind model introduced are shown in Figure 25. They indicate wind magnitudes < 8 m/s below 50 km (auxiliary scale). The winds are oscillatory above ~ 28 km, which is near the lower altitude limit of the deep stable layer (Figure 17). Hence, it is suggested that the principal meridional motions at the north probe site are oscillatory in nature and, since they occur in a stable region of the atmosphere, that they are probably a result of gravity waves. (See also Figures 14 and 15.) Below 28 km, the Doppler residuals were still somewhat randomly oscillatory, with smaller amplitudes, typically ± 2 Hz, or ± 0.3 m/s.

More information remains to be gained from analysis of the Doppler wind data. In addition there is some information in the descent velocity data which may yield vertical flow velocities. Preliminary study indicates that vertical flows ~ 0.5 m/s may be present in the lower atmosphere. These data will be studied further.

DYNAMICAL INFERENCES AND CYCLOSTROPHIC BALANCE

Several qualitative dynamical inferences can be drawn from the stability profiles. Convective overturning may occur in the middle cloud and between ~ 20 and 26 km, but everywhere else small scale convection is suppressed. Neither is shear driven instability indicated, as Richardson numbers calculated from the measured zonal winds are generally much greater than unity, with the possible exceptions of the specific regions mentioned above. Gravity waves are probably present in the stable layer above ~ 30 km. Evidence for atmospheric oscillations which we interpret as gravity waves comes from the north probe one-way Doppler residuals, Figure 25, and from probe to probe contrasts in pressure and temperature, Figures 14 and 15. These oscillatory motions have vertical wavelengths of 10 to 15 km and are essentially confined to the stable region of the atmosphere (i.e., above ~ 30 km). The magnitude of the oscillatory motion along the line of sight corresponds to $\sim +4$ to -8 m/s below 50 km altitude. The regions of local maxima in the stability indicate the possibility of trapping of gravity waves (in this connection see *Woo et al.* [this issue]). For more detailed discussions we refer the reader to *Schubert et al.* [this issue].

The qualitative features of the pressure contrasts between the probes (Figure 7) are still essentially the same as reported in *Seiff et al.* [1979b]. Quantitatively, the pressure differences have tended to be reduced as a result of refinements to the data. An enlarged plot of pressures at the cloud levels is given in Figure 26 to display better the measured differences.

If, following *Seiff et al.* [1979b], we interpret the pressure differences between the north and day probes as being consistent with a mean zonal wind in cyclostrophic balance, we compute the zonal velocities given in Figure 27. Velocities calculated from north-night differences would be comparable, but slightly (up to 10%) greater near 60 km. Below 61 km, the pressure (or altitude) differences are derived from p and T measured during low-speed descent of the probes. Above 65 km, the contrasts are derived from accelerometer data taken during high speed entry (Figure 11). Note we have assumed hemispheric symmetry so that we can take differences involving the day probe with the north probe; also we have assumed as a first approximation good to within $\pm 15\%$ [cf. *Suomi, 1974; Counselman et al.*, this issue] that the mean zonal

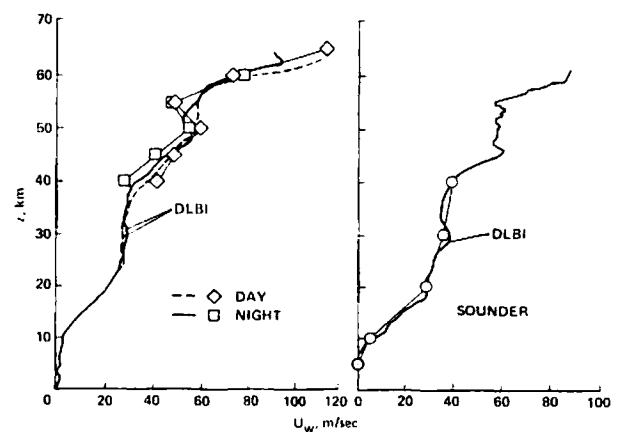


Fig. 24. Zonal winds derived from the Doppler data with trajectory analysis compared to DLBI zonal winds for the day, night, and sounder probes.

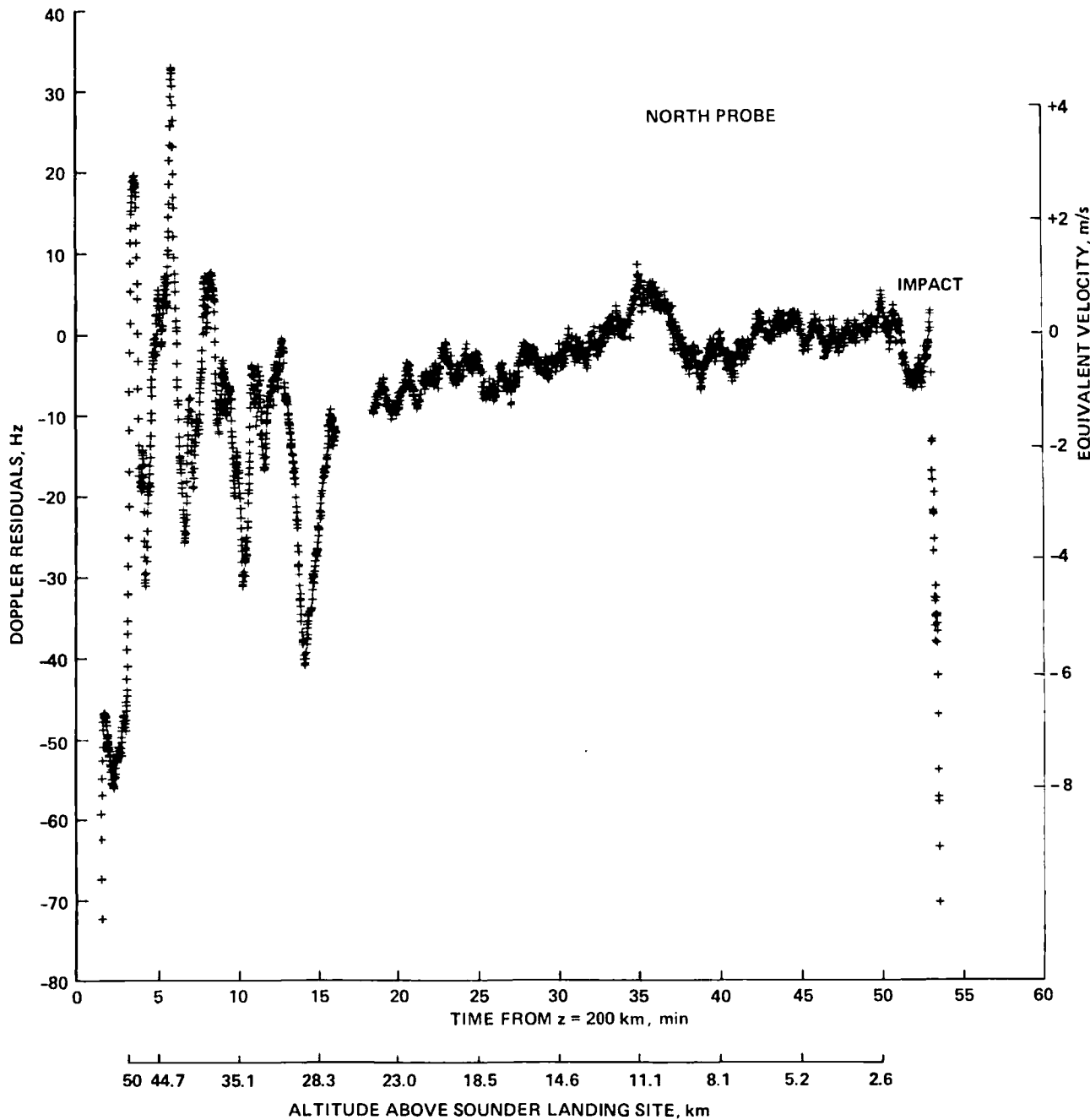


Fig. 25. North probe Doppler residuals, without winds. An oscillatory motion of the probe is indicated for altitudes between 28 and 50 km.

wind \bar{u} is constant at cloud levels between the equator and 60° latitude. Cyclostrophic balance then gives

$$(\bar{u})^2 = g\Delta z / (\ln \sin \theta)_\theta \theta^2 \quad (11)$$

where Δz is the altitude difference on a constant pressure surface, and θ is colatitude.

The computed wind profile is compared to the profiles below ~60 km for the day and north probes as measured by the DLBI experiment [Counselman et al., this issue]. The computed winds are seen to be within the range of the measurements. Above 60 km the pressure and temperature contrasts imply the zonal wind reaches a maximum of ~155 m/s near

68 km, above which it decreases and remains between 120 and 140 m/s over the altitude range 75–95 km, and then decreases again. We have terminated the wind profile near 105 km to be certain that the effects of assumed initial conditions near 120 km are of no influence on the profile. However uncertainties in probe velocity, flight path angle, etc., introduce formal uncertainties in the computed winds above 60 km, which we roughly estimate could be as large as 40%, in addition to which there may be errors related to our assumption about the latitudinal dependence of \bar{u} and perhaps the validity of cyclostrophic balance. Nevertheless, the wind profile between 70 and 90 km appears approximately consistent with that derived

1000
800
600
400
200
100
80
60
50
Fig.
at alti
sured
from
the O
of \bar{u} a
shown
this is
The
day o
clostr
latitud
der p
throug
of the
~20 k
Counse
sure o
merid
pared
1980].
tions
tions
merid

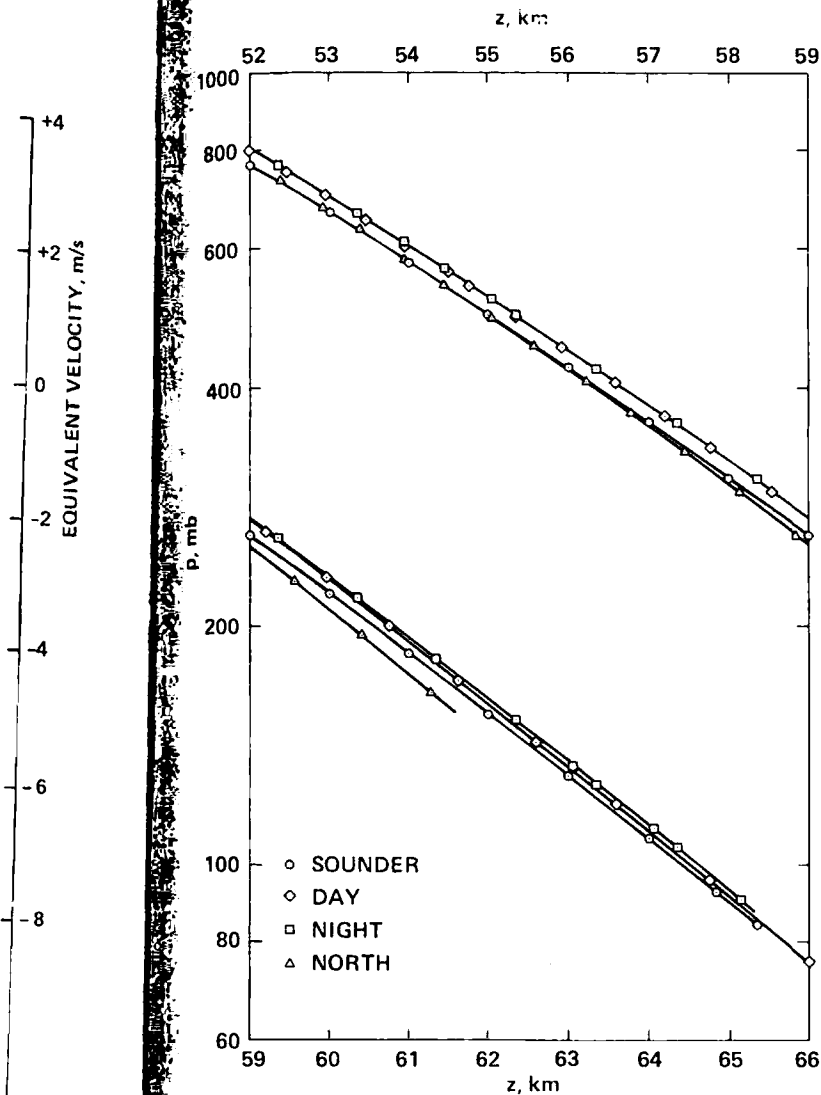


Fig. 26. Pressures from the descent data profiles of the four probes at altitudes above 52 km, plotted to an enlarged scale to show measured pressure differences.

from the zonally averaged temperature fields determined by the OIR experiment [Taylor *et al.*, this issue], given the value of \bar{u} at 70 km and the assumption of cyclostrophic balance, as shown by the curve labeled 'from OIR $T(p)$ ' [Schubert *et al.*, this issue].

The pressure contrast between the sounder and either the day or night probes in Figure 26 is not consistent with cyclostrophic balance since the day and night probes (near 30° latitude) have systematically higher pressures than the sounder probe at 4° latitude. Since this tendency has persisted throughout the data analysis, and is consistent with the sense of the meridional velocity being toward the equator above ~ 20 km for both the night and day probes, as observed by Counselman *et al.* [this issue], we believe the sense of the pressure contrasts to be real. This being the case, and since mean meridional motions are expected to be very small when compared to the mean zonal wind [cf. Suomi, 1974; Rossow *et al.*, 1980], one is led to the conclusion that nonaxisymmetric motions are present at latitudes $< 30^\circ$ which produce accelerations which are as important as the cyclostrophic term in the meridional momentum equation.

CONCLUDING REMARKS

The Pioneer Venus mission has provided many insights into the structure of the atmosphere of Venus but, needless to say, there are questions remaining and regions of the atmosphere yet to be explored. For example, the contrasts in the lower atmosphere now appear to be principally a function of latitude, but only one sounding of the full depth of the atmosphere has been made at latitudes greater than 30° , and none at latitudes greater than 60° . The thermal contrast between low latitudes and the deep polar atmosphere could provide key indications of the general circulation, for example, whether the meridional flow extends to polar latitudes, and the possibility of a polar vortex. The midday and evening atmospheric contrasts with the nightside atmosphere also require further definition, since the present indications, based on comparisons of Venera 9, 10, and Pioneer Venus results, are that they are larger than would be expected either theoretically or from measured nightside contrasts.

The observed atmospheric contrasts between the equatorial region and mid-latitudes, as seen by both Pioneer Venus and Venera 9 and 10, are in a somewhat unexpected sense, being cooler near the equator. This probably requires further investigation, and, if it occurs generally, dynamical interpretation. It is not clear, for example, whether or not this is an eddy phenomenon, which it could well be.

The possibility of sizeable temporal variations in the atmosphere also is raised by the Venera probe data, and needs to be resolved.

A surprising finding of the Pioneer Venus mission is that much of the lower and middle atmosphere of Venus (up to 120 km) is stably stratified, except for the following limited regions: in the middle cloud, between 50 and 55 km; between 20 and 30 km; and probably near the surface (below 10 km). This latter region was not measured by Pioneer Venus, but is based on our interpretation of Venera 10, and requires further confirmation. The deep stable layer just below the clouds is apparently explained by radiative equilibrium considerations, and places constraints on cloud models and water vapor content of the atmosphere. The stable atmosphere above the

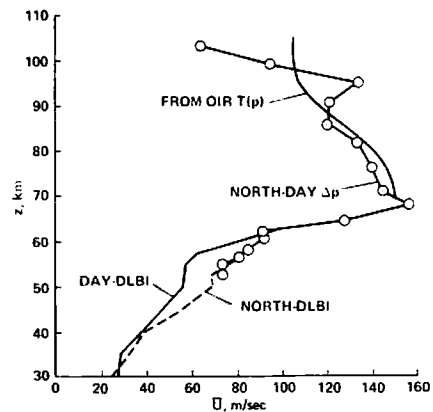


Fig. 27. Zonal wind velocities derived from measured pressure differences with the assumption of cyclostrophic balance. Pressure differences below 61 km are from the descent data, Figure 26; those above 61 km are from the entry data, Figure 11. The curve labeled OIR $T(p)$ was derived by Covey and Schubert [Schubert *et al.*, this issue] by use of the OIR data [Taylor *et al.*, this issue], the assumption of cyclostrophic balance, and an initial wind velocity of 150 m/s at 70 km altitude taken from our present work.

clouds also is in radiative equilibrium. The stability of the deeper atmosphere between 10 and 20 km is less easy to explain, and its explanation will probably lead to dynamical and/or chemical insights, in prescribing the general circulation or the absorbing species which are needed to model it. This layer is also more location dependent than the others, varying significantly from probe site to probe site, and leading to unexpectedly large contrasts in the deep atmosphere. Do these large contrasts have dynamical importance, or are they transient in nature?

Several indications were obtained of waves in the lower and middle atmosphere. One system resides in the deep subcloud stable layer, and was indicated by mass motions and by temperature and pressure oscillations. It is apparently global in extent. Its exact nature needs to be clarified. The second system arises above 110 km, continues to at least 170 km, and is of very large amplitude. We suggest that it may be excited by flow through the large, almost discontinuous jumps in density and temperature seen in the upper atmosphere at the terminators [Keating *et al.*, 1979a, b], although it could also be a thermal tide driven from below. Theoretical studies are needed to evaluate these possibilities.

An initial indication has been obtained of wind velocities above the clouds to 100 km. This indication must be regarded as indirect and tentative, but it is the only evidence presently available, and requires confirmation.

Finally, an altitude region which was not intensively investigated by Pioneer Venus is pointed out. This is above 120 km to ~145 km, above the threshold of the probe entry experiments and the orbiter IR soundings, and below the orbiter periapses, where in situ measurements were made. The bus penetrated this region down to 130 km, where the pressure became too high for the mass spectrometer to operate, and the nearby day probe reached up to 126 km to provide, effectively, one sounding through this region. This set of data indicated a region of large amplitude oscillations in temperature and density. The mean temperature structure within it does not appear to be seriously in doubt, but it would be desirable to have more than a single sounding through the layer, to see if there are variations within it diurnally or with latitude, and to further define the temperature oscillations. The homopause also is within this region [von Zahn *et al.*, this issue].

These are just a few of the areas in which future research will further our knowledge of the structure and dynamics of the atmosphere of Venus.

REFERENCES

- Avdueski, V. S., *et al.*, Automatic stations Venera 9 and Venera 10—Functioning of descent vehicles and measurement of atmospheric parameters, *Cosmic Res.*, Engl. Transl., 14, 577–592, 1976.
- Blamont, J., and B. Ragent, Further results of the Pioneer Venus nephelometer experiment, *Science*, 205, 67–70, 1979.
- Colin, L., The Pioneer Venus program, *J. Geophys. Res.*, this issue.
- Counselman, C. C., III, S. A. Gourevitch, R. W. King, and G. B. Lorient, Venus winds are zonal and retrograde below the clouds, *Science*, 205, 85–87, 1979.
- Counselman, C. C., III, S. A. Gourevitch, R. W. King, G. B. Lorient, and E. S. Ginsberg, Zonal and meridional circulation of the lower atmosphere of Venus determined by radio interferometry, *J. Geophys. Res.*, this issue.
- Hanel, R., *et al.*, Infrared observations of the Jovian System from Voyager 1, *Science*, 204, 972–976, 1979.
- Hilsenrath, J., C. W. Beckett, W. S. Benedict, L. Fano, H. J. Hoge, J. F. Musi, R. L. Nuttall, and Y. S. Touloukian, *Tables of Thermodynamic and Transport Properties of Air, Argon, Carbon Dioxide, Carbon Monoxide, Hydrogen, Nitrogen, Oxygen, and Steam*, Pergamon, New York, 1960.
- Hoffman, J. H., V. I. Oyama, and U. von Zahn, Measurements of the Venus lower atmosphere composition: A comparison of results, *J. Geophys. Res.*, this issue.
- Howard, H. T., *et al.*, Venus: Mass, gravity field, atmosphere, and ionosphere as measured by the Mariner 10 dual-frequency radio system, *Science*, 183, 1297–1301, 1974.
- Keating, G. M., R. H. Tolson, and E. W. Hinson, Venus thermosphere and exosphere: First satellite drag measurements of an extraterrestrial atmosphere, *Science*, 203, 772–774, 1979a.
- Keating, G. M., F. W. Taylor, J. Y. Nicholson, and E. W. Hinson, Short-term cyclic variations and diurnal variations of the Venus upper atmosphere, *Science*, 205, 62–64, 1979b.
- Keating, G. M., J. Y. Nicholson III, and L. R. Lake, Venus upper atmosphere structure, *J. Geophys. Res.*, this issue.
- Kliore, A. J., and I. R. Patel, The vertical structure of the atmosphere of Venus from Pioneer Venus radio occultations, *J. Geophys. Res.*, this issue.
- Knollenberg, R. G., and D. M. Hunten, Clouds of Venus: Particle size distribution measurements, *Science*, 203, 792–795, 1979.
- Kuzmin, A. D., and M. Ya. Marov, *Physics of the Planet Venus*, Nauka, Moscow, 1974.
- Marov, M. Ya., V. S. Avdueskiy, N. F. Borodin, A. P. Ekonomov, V. V. Kerzhanovich, V. P. Lysov, B. Ye. Moshkin, M. K. Rozhdzhestvenskiy, and O. L. Ryabov, Preliminary results on the Venus atmosphere from the Venera 8 descent module, *Icarus*, 20, 407–421, 1973.
- Moroz, V. I., B. E. Moshkin, A. P. Ekonomov, N. F. San'ko, N. A. Parfent'ev, and Yu. M. Golovin, Spectrometric experiment on board the Venera-11, 12 descenders: Some results of the analysis of the Venus day-side spectrum, report, Space Res. Inst., USSR Acad. of Sci., Moscow, 1979.
- Muhleman, D. O., T. Clancy, G. R. Knapp, and T. G. Phillips, The carbon monoxide distribution in the Venus atmosphere from 230 ghz spectral measurements (abstract), *Bull. Am. Astron. Soc.*, 11(3), paper 1.20, 1979.
- Niemann, H. B., R. E. Hartle, A. E. Hedin, W. T. Kasprzak, N. W. Spencer, D. M. Hunten, and G. R. Carignan, Venus upper atmosphere neutral gas composition: First observations of the diurnal variations, *Science*, 205, 54–56, 1979.
- Niemann, H. B., W. T. Kasprzak, A. E. Hedin, D. M. Hunten, and N. W. Spencer, Mass spectrometric measurements of the neutral gas composition of the thermosphere and exosphere of Venus, *J. Geophys. Res.*, this issue.
- Nier, A. O., and M. B. McElroy, Composition and structure of Mars' upper atmosphere: Results from the neutral mass spectrometers on Viking 1 and 2, *J. Geophys. Res.*, 82(28), 4341–4349, 1977.
- Oyama, V. I., G. C. Carle, F. Woeller, J. B. Pollack, R. T. Reynolds, and R. A. Craig, Composition of the Venus lower atmosphere from the Pioneer Venus gas chromatograph, *J. Geophys. Res.*, this issue.
- Pettengill, G. H., E. Eliason, P. G. Ford, G. B. Lorient, H. Masursky, and G. E. McGill, Pioneer Venus radar results: Altimetry and surface properties, *J. Geophys. Res.*, this issue.
- Pitts, W. C., and R. M. Wakefield, Performance of entry heat shields on Pioneer Venus probes, *J. Geophys. Res.*, this issue.
- Pollack, J. B., and R. E. Young, Calculations of the radiative and dynamical state of the Venus atmosphere, *J. Atmos. Sci.*, 32, 1025–1037, 1975.
- Pollack, J. B., O. B. Toon, and R. Boese, Greenhouse models of Venus' high surface temperature, as constrained by Pioneer Venus measurements, *J. Geophys. Res.*, this issue.
- Rossov, W. B., A. D. Del Genio, S. S. Lemaie, and L. D. Travis, Cloud morphology and motions from Pioneer Venus images, *J. Geophys. Res.*, this issue.
- Schubert, G., *et al.*, Structure and circulation of the Venus atmosphere, *J. Geophys. Res.*, this issue.
- Seiff, A., and D. B. Kirk, Structure of the atmosphere of Mars in summer at mid-latitudes, *J. Geophys. Res.*, 82(28), 4364–4378, 1977.
- Seiff, A., D. E. Reese, S. C. Sommer, D. B. Kirk, E. E. Whiting, and H. B. Niemann, PAET, an entry probe experiment in the earth's atmosphere, *Icarus*, 18(4), 525–563, 1973.
- Seiff, A., D. B. Kirk, S. C. Sommer, R. E. Young, R. C. Blanchard, D. W. Juergens, J. E. Lepetich, P. F. Intrieri, J. T. Findlay, and J. S. Derr, Structure of the atmosphere of Venus up to 110 kilometers:

- Preliminary results from the four Pioneer Venus entry probes, *Science*, 203, 787-790, 1979a.
- Seiff, A., D. B. Kirk, R. E. Young, S. C. Sommer, R. C. Blanchard, J. T. Findlay, and G. M. Kelly, Thermal contrast in the atmosphere of Venus: Initial appraisal from Pioneer Venus probe data, *Science*, 205, 46-49, 1979b.
- Seiff, A., D. W. Juergens, and J. E. Lepetich, Atmosphere structure instruments on the four Pioneer Venus entry probes, *IEEE Trans. Geosci. Remote Sensing*, GE-18(1), 105-111, 1980.
- Staley, D. O., The adiabatic lapse rate in the Venus atmosphere, *J. Atmos. Sci.*, 27, 219-223, 1970.
- Stone, P. H., The structure and circulation of the deep Venus atmosphere, *J. Atmos. Sci.*, 31, 1681-1690, 1974.
- Stone, P. H., The dynamics of the atmosphere of Venus, *J. Atmos. Sci.*, 32, 1005-1016, 1975.
- Suomi, V., Cloud motions on Venus, *NASA Spec. Publ.*, 382, 1974.
- Suomi, V. E., L. A. Stromovsky, and H. E. Revercomb, Preliminary results of the Pioneer Venus small probe net flux radiometer experiment, *Science*, 205, 82-85, 1979.
- Taylor, F. W., et al., Structure of the middle atmosphere of Venus: Infrared remote sensing from the Pioneer orbiter, *J. Geophys. Res.*, this issue.
- Tomasko, M. G., L. R. Doose, and P. H. Smith, Absorption of sunlight in the atmosphere of Venus, *Science*, 205, 80-82, 1979.
- von Zahn, U., D. Krankowsky, K. Mauersberger, A. O. Nier, and D. M. Hunten, Venus thermosphere: In situ composition measurements, the temperature profile, and the homopause altitude, *Science*, 203, 768-770, 1979.
- von Zahn, U., K. H. Fricke, D. M. Hunten, D. Krankowsky, K. Mauersberger, and A. O. Nier, The upper atmosphere of Venus during morning conditions, *J. Geophys. Res.*, this issue.
- Wilson, W. J., and M. J. Klein, Carbon monoxide distribution in the Venus stratosphere from 2.6 mm measurements (abstract), *Bull. Am. Astron. Soc.*, 11,(3), paper 1.21, 1979.
- Woo, R., J. W. Armstrong, and W. B. Kendall, Measurements of the turbulence in the Venus atmosphere deduced from Pioneer Venus multiprobe radio scintillations, *Science*, 205, 87-89, 1979.
- Woo, R., J. W. Armstrong, and A. Ishimaru, Radio occultation measurements of turbulence in the Venus atmosphere by Pioneer Venus, *J. Geophys. Res.*, this issue.

(Received December 27, 1979;
revised May 20, 1980;
accepted May 21, 1980.)